



## Improving predictability of high ozone episodes through dynamic boundary conditions, emission refresh and chemical data assimilation during the Long Island Sound Tropospheric Ozone Study (LISTOS) field campaign

5

Siqi Ma<sup>1,2</sup>, Daniel Tong<sup>1,3\*</sup>, Lok Lamsal<sup>4,5</sup>, Julian Wang<sup>6\*</sup>, Xuelei Zhang<sup>3</sup>, Youhua Tang<sup>3,6</sup>, Rick Saylor<sup>6</sup>, Tianfeng Chai<sup>4</sup>, Pius Lee<sup>6</sup>, Patrick Campbell<sup>3,6</sup>, Barry Baker<sup>3,6</sup>, Shobha Kondragunta<sup>7</sup>, Laura Judd<sup>8</sup>, Timothy A. Berkoff<sup>8</sup>, Scott J. Janz<sup>4</sup>, and Ivanka Stajner<sup>9</sup>

<sup>1</sup>Department of Atmospheric, Oceanic and Earth Sciences, George Mason University, Fairfax, VA 22030 USA

10 <sup>2</sup>National Research Council, hosted by the National Oceanic and Atmospheric Administration Air Resources Lab, College Park, MD 20740 USA

<sup>3</sup>Center for Spatial Information Science and Systems, George Mason University, Fairfax, VA 22030 USA

<sup>4</sup>Atmospheric Chemistry and Dynamics Laboratory, NASA Goddard Space Flight Center, MD 20771 USA

<sup>5</sup>Universities Space Research Association, Columbia, MD 21046 USA

15 <sup>6</sup>National Oceanic and Atmospheric Administration (NOAA) Air Resources Laboratory, College Park, MD 22030 USA

<sup>7</sup>NOAA National Environmental Satellite Data and Information Service, College Park, MD 20740 USA

<sup>8</sup>NASA Langley Research Center, Hampton, VA, 23681 USA

<sup>9</sup>NOAA National Weather Service National Centers for Environmental Prediction, College Park, MD 20740 USA

Corresponding authors: Daniel Tong (qtong@gmu.edu); Julian Wang (julian.wang@noaa.gov)

20 **Abstract.** Although air quality in the United States improved remarkably in the past decades, ground-level ozone (O<sub>3</sub>) rises often in exceedance of the national ambient air quality standard in nonattainment areas, including the Long Island Sound (LIS) and its surrounding areas. Accurate prediction of high ozone episodes is needed to assist government agencies and the public in mitigating harmful effects of air pollution. In this study, we have developed a suite of potential forecast improvements, including dynamic boundary conditions, rapid emission refresh and chemical data assimilation, 25 in a 3 km resolution Community Multi-scale Air Quality (CMAQ) modeling system. The purpose is to evaluate and assess the effectiveness of these forecasting techniques, individually or in combination, in improving forecast guidance for two major air pollutants: surface O<sub>3</sub> and nitrogen dioxide (NO<sub>2</sub>). Experiments were conducted for a high O<sub>3</sub> episode (August 28–29, 2018) during the Long Island Sound Tropospheric Ozone Study (LISTOS) field campaign, which provides abundant observations for evaluating model performance. The results show that these forecast system updates are useful 30 in enhancing the capability of the forecasting model with varying effectiveness for different pollutants. For O<sub>3</sub> prediction, the most significant improvement comes from the dynamic boundary conditions derived from NOAA National Air Quality Forecast Capability (NAQFC), which increases the correlation coefficient (R) from 0.81 to 0.93 and reduces the Root Mean Square Error (RMSE) from 14.97 ppbv to 8.22 ppbv, compared to that with the static boundary conditions. 35 The NO<sub>2</sub> from all high-resolution simulations outperforms that from the operational 12 km NAQFC simulation, highlighting the importance of spatially resolved emission and meteorology inputs for the prediction of short-lived pollutants. The effectiveness of improved initial concentrations through optimal interpolation (OI) is shown to be high in urban areas with high emission density. The influence of OI adjustment, however, is maintained for a longer period in rural areas where emissions and chemical transformation make a smaller contribution to the O<sub>3</sub> budget than that in high emission areas. Following the assessment of individual forecast system updates, the forecasting system is configured with 40 dynamic boundary conditions, optimal interpolation of initial concentrations, and emission adjustment, to simulate the



high ozone episode over the Long Island Sound region. The newly developed forecasting system significantly reduces the bias of surface  $\text{NO}_2$  concentration. When compared with the NASA Langley GeoCAPE Airborne Simulator (GCAS) vertical column density (VCD), the new system is able to reproduce the  $\text{NO}_2$  VCD with a higher correlation (0.74), lower normalized mean bias (40%) and normalized mean error (61%) than NAQFC (0.57, 45% and 76%, respectively). The new system captures magnitude and timing of surface  $\text{O}_3$  peaks and valleys better. In comparison with LIDAR  $\text{O}_3$  profile variability of the vertical  $\text{O}_3$  is captured better by the new system (correlation coefficient of 0.71) than by NAQFC (correlation coefficient of 0.54). Although the experiments are limited to one pollution episode over the Long Island Sound, this study demonstrates feasible approaches to improve the predictability of high  $\text{O}_3$  episodes in contemporary urban environments.

## 50 1. Introduction

Exposure to ambient air pollutants has been associated with detrimental health effects, including cardiovascular diseases and premature deaths (Brunekreef and Holgate, 2002; Kim, 2007; Héroux et al., 2015). Recent decades saw remarkable improvement in the air quality across the United States. From 1990 to 2015, the United States Environmental Protection Agency (US EPA) estimated that the emissions of nitrogen oxides ( $\text{NO}_x$ ), a major pollutant that controls regional ozone formation, were reduced from 25.2 to 11.5 million  $\text{t yr}^{-1}$  (Feng et al., 2020). The downward trends in  $\text{NO}_x$  emissions have been verified by ground and satellite observations in large cities (Tong et al., 2015) and in the eastern United States (Zhou et al., 2013; Krotkov et al., 2016). Because of the substantial emission reductions, ground-level ozone concentrations decreased ubiquitously across the US (Hogrefe et al., 2011; Simon et al., 2015; He et al., 2020).

Regardless of the tremendous improvement in air quality, more than one third of the US population still lives in areas exceeding the National Ambient Air Quality Standards (NAAQS) for ozone ( $\text{O}_3$ ) and/or fine particulate matter ( $\text{PM}_{2.5}$ ) (US EPA, 2020). Many of these ozone nonattainment areas are located along the northeastern Interstate 95 (I-95, Interstate Highway on the East Coast of the United States) corridor where high density of emissions is produced by transportation and other industrial sources. Surface ozone is formed from photochemical reactions between  $\text{NO}_x$  and volatile organic compounds (VOCs) (NRC, 1992), and the high emission density of  $\text{NO}_x$  is a major controlling factor for high ozone events in this region.

As part of the efforts to understand regional  $\text{O}_3$  pollution, a multi-agency collaborative study of precursor emissions, ground-level  $\text{O}_3$  formation and transport in the New York City (NYC) metropolitan region and downwind locations, the Long Island Sound Tropospheric Ozone Study (LISTOS), was launched. Extensive measurements were collected between June and September 2018 within the NYC metropolitan area and over Long Island Sound (LIS). Several studies have been conducted to investigate the spatial and vertical variability of  $\text{O}_3$  and its precursors using numerical models and observations collected during the LISTOS field campaign (Baker et al., 2019; Shu et al., 2019; Berkoff et al., 2019).

Air quality forecasts are a critical tool used by environmental and public health agencies to mitigate the detrimental effects of air pollution (Tong and Tang, 2018). Accurate prediction of ambient ozone and its precursors remains challenging due to inherent uncertainties in the model processes (transport, chemistry and removal), as well as in model inputs such as emissions, initial concentrations (ICs) and boundary conditions (BCs). Prior studies have also revealed that air quality models face additional challenges in predicting surface  $\text{O}_3$  concentrations at coastal locations or over complex



urban areas (e.g., Tong et al., 2006; Hogrefe et al., 2007). Therefore, several modeling techniques have been developed to improve the forecasting skills of these air quality models (Liu et al., 2001; Tang et al., 2007). Previous studies (Wu et al., 2008; Sandu et al., 2010) suggested employing data assimilation methods to adjust the initial conditions of a model to reduce model bias. Optimal interpolation (OI) is a simple data assimilation method used to enhance model prediction (Candiani et al., 2013; Tang et al., 2015; Tang et al., 2017). Considering the modeling sensitivity to BCs, Tang et al. (2009) examined the impact of six types of lateral BCs on the CMAQ (Community Multiscale Air Quality) forecast ability and the results showed that using global model predictions for BCs was able to improve the correlation coefficients of surface O<sub>3</sub> prediction compared to observations. Evaluations of different databases and configurations for BCs in short-term and long-term simulations also showed that dynamic BCs could have a positive impact on numerical predictions (Tang et al., 2007; Makar et al., 2010; Henderson et al., 2014; Khan and Kumar, 2019). However, many of these studies used BCs based on global forecasts that had a relatively low resolution (e.g. 1.4° × 1.4° and 2° × 2.5°). Therefore, databases with higher resolution, such as satellite observations or regional forecasting products, were introduced to construct boundary conditions that were shown to result in a measurable improvement in model performance (Borge et al., 2010; Pour-Biazar et al., 2011). Finally, updating emissions from the base year to the specific forecast year was shown to be an effective approach to reduce the uncertainties of outdated emission inventories to increase forecasting accuracy (Pan et al., 2014; Tong et al., 2015, 2016).

This study examines to what extent can various modeling techniques improve O<sub>3</sub> and NO<sub>2</sub> predictions over LIS and surrounding areas. As the largest metropolitan area in the United States on the Atlantic Ocean coast, this LIS region represents one of the most challenging places for air quality modeling. To better resolve fine-scale processes such as sea breeze and recirculation of air pollutants at coastal sites, a high-resolution air quality forecasting system (3 km) is developed using the latest meteorology and air quality models. Using observations from ground air quality monitors and the LISTOS field campaign, we evaluate the forecasting skills of the high-resolution air quality forecasting system to predict O<sub>3</sub> and NO<sub>2</sub> over LIS. Specifically, we use three forecast improvements - dynamic boundary conditions, rapid emission refresh, and chemical data assimilation - to improve the newly developed system. The effectiveness of each technique to improve forecasting skill is assessed using the observations from the LISTOS and the EPA AirNow network (<http://airnowapi.org>). Descriptions of the modeling system, forecast improvements, and observation data are presented in Section 2. Assessments of the CMAQ results with and without different forecast system updates are described in Section 3. A summary of our findings and concluding remarks are provided in Section 4.

105

## 2. Methodology

### 2.1 Study design

To simulate ozone variability over a complex coastal urban environment, a high-resolution air quality forecasting system has been developed for LIS and surrounding areas. The forecasting system is comprised of state-of-the-science weather, emission, and chemical transport models. The model domain covers eastern Pennsylvania, New Jersey, southern New York, Connecticut and Rhode Island. Even though this domain is large enough to capture fine scale processes, the

110



influence of regional transport cannot be adequately represented. Therefore, real-time forecasts from the operational National Air Quality Forecast Capability (NAQFC), produced by the NOAA National Weather Service, are used to provide dynamic boundary conditions to investigate the effect of this model input on forecasting performance. We also  
115 explore the effects of emission adjustment and chemical data assimilation on forecasting performance.

Five groups of simulations are designed to evaluate the performance and effectiveness of different adjustments of the CMAQ model (Table 1). The Control run uses no adjustment by using default profile as BCs. The second experiment, named as BCON, is similar to the Control run, except that dynamic boundary conditions from the NOAA NAQFC were  
120 applied to replace the default BCs. In the Optimal Interpolation (OI) run, the initial concentrations in CMAQ are adjusted with three observation interpolation methods, including area-average (OI\_avg), inverse distance weighing (idw), and CMAQ concentration gradients (OI\_bias). The best performer of these approaches will be used in the subsequent analyses. Next, a group of emission adjustment experiments are designed to update NO<sub>x</sub> emissions using observed changes from satellite and ground sensors (Tong et al., 2016). These emission adjustment factors are applied either uniformly across  
125 the domain (EmisAdj\_whole), or separately for each subdomain (EmisAdj\_sub). In the latter case, the domain was divided into five regions based on city areas: New York City (NYC), City of Philadelphia (PH), city area of New Haven-Hartford (NHH) and Providence-Pawtucket (PP), and the area other than these four regions (OTHR) (Fig. 1). Finally, two simulations with the combinations of these three techniques were conducted in search of the best performer. All simulations were conducted for a high ozone episode, which lasted 168 hours from 0:00Z August 25th to 23:00Z August  
130 31th, 2018.

## 2.2 High-resolution air quality forecasting system

The high-resolution air quality forecasting system used here is comprised of three major components: meteorology, emission, and chemical transport models. The Weather Research and Forecasting (WRF) model version 4.0 (Skamarock et al., 2019) is used to generate hourly meteorological fields to drive emission and air quality modeling. The WRF model  
135 was configured with Thompson graupel microphysics scheme, RRTMG long and short-wave radiation scheme, Mellor-Yamada-Janjic PBL scheme, unified Noah land-surface model and Tiedtke cumulus parameterization option. There are 41 vertical layers with 20 layers below 1 km and top layer at 50 hPa. The Global Forecast System (GFS) version 4 products with a horizontal resolution of  $0.25^\circ \times 0.25^\circ$  (available every 6 h) were employed to drive the WRF model.

The emission input was provided using a hybrid emission modeling system that utilized the Sparse Matrix Operator Kernel Emissions (SMOKE) model (Houyoux et al., 2000) version 4.7 to process recurring anthropogenic emissions, and a suite of emission models to estimate emissions from intermittent and/or meteorology-dependent sources. Anthropogenic emissions from area and mobile sources were taken from US EPA 2011 NEI version 2 (NEI2011v2). The Motor Vehicle Emissions Simulator (MOVES) was used to generate county-level emission factors for the onroad and offroad sources. SMOKE uses a combination of vehicle activity data, MOVES emission factors, meteorology and other ancillary data  
145 (spatial, temporal and speciation information) to generate hourly speciated model-ready emission data. Point sources were processed in two steps. In the first step, emission inventories of point sources were processed with SMOKE to generate intermediate input files. Next, these intermediate files were used to drive inline calculation of plume rise to distribute point source emissions vertically in the CMAQ model domain. Two natural sources are included in this forecasting system:



150 biogenic and sea-salt. Biogenic emissions from terrestrial plants were predicted using the inline version of the Biogenic Emission Inventory System (BEIS) (Pierce et al., 1998). The emissions of sea spray aerosols are calculated using an updated version of the Gong (2003) sea-spray emission parameterization (Gantt et al., 2015).

155 The CMAQ model ingests emissions and meteorology to predict spatial and temporal variations of O<sub>3</sub>, NO<sub>2</sub>, and their precursors. In this study, version 5.3.1 of the CMAQ model was configured to include detailed implementation of inline emission processes for biogenic, sea-salt and elevated anthropogenic emissions, horizontal and vertical advection, turbulent diffusion, dry/wet deposition and full gas, aqueous and aerosol chemistry using a revised Carbon Bond 6 gas-phase mechanism and AE6 aerosol mechanism (CB6r3\_AE6\_AQ) (Byun and Schere, 2006; Luecken et al., 2019). Both the meteorological and air quality models have a 3 km horizontal resolution over the LIS region and its surrounding areas (Fig. 1).

### 2.3 Techniques to improve forecasting skills

160 We implement and test three forecasting improvement techniques to assess their effectiveness in enhancing the simulation performance of the CMAQ model. Details of each update are described below.

#### *a) Dynamic lateral boundary conditions*

165 Regional air quality models such as CMAQ rely on lateral boundary conditions to account for inflow of air pollutants and precursors from out-of-domain sources. These boundary conditions fall into two categories: static and dynamic. Static boundary conditions are time-independent vertical profiles of appropriate species at the boundaries that can be prepared from prescribed profiles, long-term vertical observations, or climatological model simulations (Tong and Mauzerall, 2006; Tang et al., 2007). Dynamical boundary conditions are provided by a concurrently running global model or another regional model covering a larger domain. We compare here two sets of boundary conditions: the static boundary conditions created using the default CMAQ profiles, and the dynamic boundary conditions derived from the NOAA  
170 National Air Quality Forecast Capability (NAQFC). Hourly forecasts of the NAQFC (Lee et al., 2017), operated by the National Weather Services, are processed using the BCON tool developed by the US EPA.

#### *b) Optimal Interpolation*

175 Optimal Interpolation (OI) is a commonly applied data assimilation method (Wang et al., 2013; Chai et al., 2017) that can be used to adjust the initial conditions (ICs) of an air quality model to minimize errors (Adhikary, 2008). The equation of the OI method is defined as:

$$x^a = x^b + BH^T(HBH^T + O)^{-1}(y - Hx^b) \quad (1)$$

where  $x^a$  and  $x^b$  are the analyzed and background fields, respectively.  $B$  and  $O$  are the background and observation error covariance matrix,  $H$  is the observational operator and  $H^T$  is its matrix transpose, and  $y$  is the observation vector.

180 To constrain the biases in ICs used by CMAQ, the concentrations of ozone, NO<sub>2</sub> and NO in the CMAQ restart file, called CGRID, were adjusted via the OI method, which is applied every 24 hours at 0:00 Coordinated Universal Time. This adjustment was made on each block of 11×11 grid cells of the surface layer over the whole domain to obtain the analyzed field  $X^a$ . Next, the ratio between  $X^a$  and  $X^b$  at each affected surface layer grid point was used to scale the concentrations for the vertical layers within the PBL. Detailed information for this method is described in Tang et al. (2015; 2017).



185 In addition to the Tang (2015) approach, two additional OI methods were included and tested for the CMAQ  
simulation. The OI assimilation first allocates ground-based observational data from the EPA AIRNow network into  
model grid cells. The Tang et al., (2015) method puts in-situ data directly into the corresponding model grid cells. If there  
was more than one active site in the same grid cell, the observations are first averaged before being applied to the grid  
cell (OI\_avg hereafter). Grid cells that did not have observations and were not within 5 grids cells from the observations  
190 were not adjusted. Experiments were also performed with two different interpolation methods. The first one was to  
interpolate the averaged observational grid points to the whole domain using the Inverse Distance Weighted (IDW)  
interpolation scheme (Shepard, 1968), (the OI\_idw method). The second method adjusted the initial concentrations by  
subtracting the bias between the simulation and the averaged observations within the grid point, then smoothing the  
adjusted concentration field via the IDW scheme. This method is called OI\_bias.

195 *c) Emission refresh*

The third forecast system update evaluated here is the rapid emission refresh capability that allows timely updates of  
outdated NEIs to the forecasting year (Tong et al., 2016). Here we focus on updating NO<sub>x</sub> emissions. NO<sub>x</sub> are important  
precursors to tropospheric ozone formation (Spicer, 1983; Chameides et al., 1992), therefore, their emissions can  
influence atmospheric ozone concentrations. Since NO<sub>x</sub> emissions decreased substantially over the last decade (Silvern  
200 et al., 2019; Dix et al., 2020) and the anthropogenic emission used in this study are based on the 2011 NEIs, the NO<sub>x</sub>  
emissions need to be projected from 2011 to the forecast year (2018). According to the approach proposed by Tong et al.  
(2016), the adjustment factor used for the emission projection is derived from the monthly changing rates of surface- and  
satellite-observed NO<sub>x</sub> (NO<sub>2</sub>). Temporal trends at the surface are determined from the hourly observed NO<sub>x</sub> concentration  
during the morning rush hours (06, 07, 08, and 09 local time). These times are optimal for assessing local emission  
205 conditions since they are related to the highest NO<sub>x</sub> levels typically produced as a result of both commuter traffic peaks  
and the shallow morning planetary boundary layer (Tong et al. 2015). Satellite-based temporal trends are calculated from  
the monthly NO<sub>2</sub> product retrieved from the Ozone Monitoring Instrument (OMI) aboard the Aura satellite (Lamsal et al.,  
2020). A weighting function is introduced to combine the surface-based and satellite-based temporal trends to acquire the  
merged projection adjustment factor (AF) for a specified region:

210 
$$AF = \frac{\Delta S \times N_S \times f_S + \Delta G \times N_G \times f_G}{N_S \times f_S + N_G \times f_G} \quad (2)$$

where  $\Delta S$  and  $N_S$  are the temporal trend and the number of satellite data, respectively; and,  $\Delta G$  and  $N_G$  are the temporal  
trend and the number of surface-based data, respectively. Two weighting factors,  $f_S$  and  $f_G$  are applied to the satellite and  
surface data, respectively. Here the value of  $f_S$  is set to 1 and  $f_G$  to 100 to avoid dominance by either data source (Tong et  
al., 2015). In this study, two groups of AFs are prepared for the emission projection. One is the average AF over the whole  
215 domain (EmisAdj\_avg) and the other group includes the AFs for each sub-region in the research area (EmisAdj\_sub).  
The AFs used in both groups are the averages of the monthly AFs from May to September. From 2011 to 2018, the change  
rate of emission (AF) is -18.6% for this model domain.

#### 2.4 Observational data sets

220 In this study, a suite of observational datasets were used either as inputs for emissions and chemical data assimilation  
or to evaluate model performance. These datasets include surface O<sub>3</sub> and NO<sub>2</sub> measurements from the US EPA Air Quality



System (AQS) surface network, the NO<sub>2</sub> vertical column density (VCD) from the Ozone Monitoring Instrument (OMI) aboard the Aura satellite, NO<sub>2</sub> VCD from the GeoCAPE Airborne Simulator (GCAS) on the NASA Langley Research Center B200 aircraft, and the O<sub>3</sub> vertical profile from the NASA Langley Mobile Ozone Lidar (LMOL). Detailed information of each data set is provided below.

225 Surface concentrations of O<sub>3</sub> and NO<sub>2</sub> are obtained from the AQS network and used for emission adjustment and chemical data assimilation, as well as evaluation of model performance. AQS is a routine monitoring network established to collect ambient air pollution data in urban, suburban, and rural areas. AQS monitors determine O<sub>3</sub> concentrations according to the Federal Reference Method promulgated in the 2015 revisions to the National Ambient Air Quality Standards (Long et al., 2014) and NO<sub>x</sub> concentrations using the chemiluminescence instruments described by McClenny  
230 et al. (2002). AQS measures both O<sub>3</sub> and NO<sub>2</sub> at hourly intervals. Note that NO<sub>2</sub> measurements are typically biased high due to interference in the chemiluminescence measurement (Dunlea et al., 2007). As the goal of this study is to improve forecasting performance, a near-real-time version of the AQS data was used, called AirNow. This is a preliminary dataset for the purpose of real-time air quality reporting and forecasting; it is not fully verified and provides fewer measured species. The data used in this study are downloaded from the AirNow data portal maintained by the US EPA  
235 (<https://files.airnowtech.org/?prefix=airnow/>).

NO<sub>2</sub> VCD measurements were provided by the Ozone Monitoring Instrument (OMI) standard product (version 4), available from the NASA Goddard Earth Sciences Data and Information Services Center (GES DISC). OMI aboard the Aura satellite is a nadir-viewing hyperspectral imaging spectrometer that measures solar backscattered radiance and solar irradiance in the ultraviolet and visible regions (270–500 nm) (Levelt et al., 2006). The Aura spacecraft has a local  
240 equator-crossing time of 13:45 h in the ascending node. OMI views the Earth along the satellite track with a swath of 3600 km on the surface in order to provide daily global coverage. In the normal global operational mode, the OMI ground pixel at nadir is approximately 13 km × 24 km, with increasing pixel sizes toward the edges of the orbital swaths. Multi-year OMI NO<sub>2</sub> data were further aggregated to calculate state-level emission adjustment factors using a mass conservation approach (Tong et al., 2015).

245 The high-resolution NO<sub>2</sub> observations from the GeoCAPE Airborne Simulator (GCAS; Kowalewski and Janz, 2014) are used for a direct comparison against model simulations of the NO<sub>2</sub> VCD. GCAS is an ultraviolet-visible spectrometer used in air quality field studies to map the spatiotemporal distribution of NO<sub>2</sub> and HCHO VCDs at high spatial resolution (Nowlan et al., 2018; Judd et al., 2019). For LISTOS, this instrument flew on 11 flight days collecting between 2-4  
250 gapless raster datasets at spatial resolutions for NO<sub>2</sub> as fine as 250 x 250 m. More information about the retrieval can be found in Judd et al. (2019). During LISTOS, NO<sub>2</sub> from GCAS was validated using coincident Pandora measurements and had a median percent difference of -1.2% with 95% of the most temporally homogeneous points within ± 25% or 0.1DU.

Finally, O<sub>3</sub> vertical profiles from the NASA Langley Mobile Ozone Lidar (LMOL) are used to evaluate the CMAQ prediction of O<sub>3</sub> profiles during the LISTOS field campaign. LMOL is part of a NASA-sponsored ozone lidar network called the tropospheric ozone lidar network (TOLNet; Sullivan et al., 2019). LMOL is a mobile ground-based ozone lidar  
255 platform equipped with a pulsed UV laser and all associated power and lidar control support units (De Young et al., 2017, Gronoff et al., 2019). In this study, we use LMOL lidar observations from Westport (41.118° N, 73.337° W). All available



field measurement parameters during this campaign were obtained from the LISTOS Data Archive (<https://www-air.larc.nasa.gov/missions/listos/index.html>).

### 3. Evaluation on the effectiveness of simulation improvements

#### 260 3.1 Effects of boundary conditions

In this section, we examine the effects of using the static and dynamic boundary conditions on O<sub>3</sub> and NO<sub>2</sub> predictions. As a reference, we also compare these simulations to the NAQFC results, extracted for the same region, during the August 29 high ozone event. Figure 2 shows the O<sub>3</sub> and NO<sub>2</sub> 24-hour average concentrations simulated by Control (static BCs), BCON (dynamic BCs) and the NOAA NAQFC over the LIS region. Ozone concentrations for the Control run ranged  
265 from 20 to 35 ppb, much lower than the observed results (30–60 ppb) over the model domain. This suggests the default profiles provided by CMAQ represent a clean environment, such as marine air layer, and are not suitable for areas with active emissions and tropospheric O<sub>3</sub> production. In comparison, the concentration level using dynamic boundary conditions increases considerably and is closer to the observations. High O<sub>3</sub> concentrations appear over near-coast areas, but are lower in the northwest of the domain. This spatial pattern illustrates the ozone river in a northeastward direction  
270 along the I-95 corridor, extending from Philadelphia to NYC, and then to Connecticut where the worst air quality is often observed. Although it overestimates surface O<sub>3</sub> in Philadelphia and central New Jersey, the BCON simulation can reproduce O<sub>3</sub> hourly variations during this episode well in comparison with the observed data (see the time series in Fig. 2d). Compared to the Control run, the BCON run performed better not only in bias, but also with higher correlations between prediction and observations (Table S1), especially during the August 26–27 high O<sub>3</sub> days.

275 The performance of the two high-resolution simulations was next compared to that by the NAQFC. The NAQFC simulation, which is being used to provide national numerical guidance for O<sub>3</sub> and PM<sub>2.5</sub> (Lee et al., 2017), is run at a coarser resolution (12 km), using a different CMAQ version (a revised CMAQ5.0), driven by different emission and meteorology datasets. Regardless of these differences, the NAQFC and BCON runs predict similar surface O<sub>3</sub> distribution patterns. Compared to the NAQFC prediction, the BCON run performs better over southern New Jersey, Long Island  
280 Sound, and northeast of the LIS domain, in particular exhibiting much-reduced biases in the LIS downwind areas. The BCON run overestimates the peak O<sub>3</sub> concentrations on August 28 and 29, while the NAQFC run performs well and is closer to the measurements. Use of coarser resolution NAQFC predictions as BCs substantially improves the capability of the 3 km forecasting system to reproduce the O<sub>3</sub> variability. Compared to the Control run, the correlation coefficient between BCON and observed O<sub>3</sub> concentrations increases from 0.81 to 0.93 and the relative mean square error (RMSE)  
285 decreases from 14.97 ppbv to 8.22 ppbv with a reduction of 45%, resulting in a comparable performance with the NOAA NAQFC predictions ( $r = 0.91$ ).

The spatial patterns of predicted NO<sub>2</sub> concentrations from the Control, BCON, and NAQFC runs are quite similar with high value areas all appearing over the NYC area (Fig. 3). This is because the NO<sub>2</sub> budget in urban areas is mainly influenced by emissions, and less by regional transport. As a result, the effect of dynamic BCs is much smaller for NO<sub>2</sub>  
290 prediction compared to O<sub>3</sub>. In addition, the simulated NO<sub>2</sub> concentrations by the 3 km forecasting system, either with static or with dynamic BCs, agree better with the observations than those from the 12 km NAQFC simulation, highlighting



the importance of using high resolution inputs to better represent the emission sources in the model. The correlation coefficient and RMSEs for the Control and BCON runs are 0.69 (4.12 ppb) and 0.71 (3.82 ppb), respectively, while those of NOAA are 0.67 (4.98 ppb) (Table S1).

### 295 3.2 Effects of initial condition adjustment

Initial concentrations are an important input to air quality forecasting. Adjusting initial concentrations through chemical data assimilation has been shown to significantly improve air quality forecasting (Tang et al., 2015; Chai et al., 2017) although the impacts wane with increasing forecast length. Here we study the effects of adjusting initial conditions on O<sub>3</sub> and NO<sub>2</sub> prediction using various OI methods. Figure 4 illustrates the initial concentrations of surface O<sub>3</sub> adjusted by OI\_avg, OI\_idw and OI\_bias, respectively. In the initial concentrations, the areas influenced by OI\_avg are primarily limited to the ground-based sites and the regions within two model grid cells in each direction of the observations (Fig. 4a). The rest of the domain is not affected by the adjustment, resulting in significant differences between adjusted and unadjusted areas. The O<sub>3</sub> fields adjusted by OI\_idw and OI\_bias show similar horizontal distributions (Fig. 4b, c), but the concentration level of OI\_bias is relatively higher over NYC and northern New Jersey. Furthermore, in contrast to the localized changes by OI\_avg, those of OI\_idw and OI\_bias show more consistent changes over larger parts of the domain.

Next, the initial concentrations files after adjustment are used to feed CMAQ simulations. The O<sub>3</sub> prediction by the Control run and three OI runs at 00Z on August 26, 2018 (the first hour after OI adjusting) are depicted in Fig. 5. The adjusted O<sub>3</sub> fields show different patterns than in the Control run with no IC adjustment. The O<sub>3</sub> field with the OI\_avg method still presents a distribution with localized high value areas near observational sites. The biases between observed and predicted concentrations are reduced in most of the areas. The RMSEs for O<sub>3</sub> are reduced from 14.97 ppbv to 13.72 ppbv in the OI\_bias run and to 14.30 in the OI\_avg run. The correlation also slightly increases from the Control to the OI runs (Table 2) for O<sub>3</sub>. In comparison, NO<sub>2</sub> prediction is less influenced by the IC adjustment, with insignificant changes in the model performance (Table 3). In addition, the effects of this adjustment on the modeling results decrease with the simulation time and display no discernible difference from the Control run after 12 hours (Fig. S1). Generally, the improvement of the simulated results due to OI data assimilation over the study domain is smaller than that from the dynamic BCs for this particular domain. Note a change in the model domain or data assimilation approach may yield different relative changes between BCs and ICs adjustments. Among the three OI methods, the simulation with OI\_bias shows the best performance, so this method is chosen for subsequent analyses in which multiple techniques are combined to improve forecasting skills. It is interesting to note that the duration of OI influence on O<sub>3</sub> simulation varies from place to place. Figure 6 shows the time series of the averaged differences in predicted hourly O<sub>3</sub> concentrations between the Control run and each of the three OI runs from August 26 to 31, 2018 in three urban areas (NYC, Philadelphia, New Haven – Hartford) and other (OTHR) areas. The differences illustrate the effect of adjusting initial concentrations on O<sub>3</sub> prediction. In large metropolitan areas, OI adjustments result in a large spike up to 14 ppbv in surface hourly O<sub>3</sub> concentrations over NYC and 16 ppbv over Philadelphia, respectively. In comparison, the spikes in non-urban areas are much smaller, reflecting the fact that there are smaller biases between observations and prediction (Fig. 6). The New Haven–Hartford region, which has an emission density between large cities and non-urban areas, sees a change of O<sub>3</sub> concentration between these two groups. The OI effects in large cities remain for a shorter time than in non-urban area or



330 smaller cities. For example, the differences between OI runs and the Control run decrease to ~0 ppb in four to eight hours in two metropolitan areas, NYC and Philadelphia (Fig. 6a, b). Meanwhile, in the New Haven – Hartford region (Fig. 6c), Providence-Pawtucket region (not shown) and the non-urban areas (Fig. 6d), the differences could last 12 to 16 hours. This difference in the impact duration reflects the dependence of O<sub>3</sub> level on the initial concentrations in the air quality model. In general, the influence of OI adjustment lingers for a longer period in an area with low emission density where emissions and chemical reactions make a smaller contribution to the O<sub>3</sub> budget than that in the area with high emission density.

### 335 3.3 Effects of NO<sub>x</sub> emission adjustment

One of the major challenges in air quality forecasting is the time lag in updating the emission inputs generated for a specified base year which is typically different than the year for which the simulation is desired (Tong et al., 2012). Here we test the effects of implementing a new emission update technique, the rapid emission refresh, on forecasting performance. In this study, the NEI2011v2 data are used to represent anthropogenic emissions, while the target forecasting year is 2018. Both the AQS ground monitors and the OMI sensor observed considerable decreases in NO<sub>x</sub> emissions during summertime (May-September) from 2011 to 2018 (Fig. 7). The largest reduction appears in the west of NYC. The OMI NO<sub>2</sub> observations show an increase primarily over Connecticut and Rhode Island, the region downwind of the Long Island Sound (Fig. 7b). The average adjustment factor (AF) for the whole domain is -18.6%. The AFs for each subdomain are -46.8% for NYC, -12.7% for Philadelphia, -10.9% for the New Haven – Hartford region, -39.5% for the Providence-Pawtucket region, and -21.1% for other regions, respectively. In general, the NO<sub>x</sub> variations in this study are similar to that between 2005 and 2012 (Tong et al., 2015), indicating that the NO<sub>x</sub> emissions continued decreasing during the past 14 years. This trend highlights the importance of updating NEIs in order to reduce the bias in the emission input to model simulations.

350 The results show that the performance for O<sub>3</sub> and NO<sub>2</sub> prediction is similar between two simulations using two emission adjustment methods (a uniform average adjustment factor over the entire domain, and spatially varied factors for each subdomain as defined in Figure 1). The correlation for both simulations is 0.81 for O<sub>3</sub> and 0.69 for NO<sub>2</sub>, respectively. The biases and errors are also at the same level from the two simulations (Table 4). Compared to the O<sub>3</sub> in the Control run, RMSE changes slightly from 14.97 ppbv to 14.71 ppbv (EmisAdj\_avg) and 14.41 ppbv (EmisAdj\_sub), while the correlation remains the same. This demonstrates that emission adjustment alone results in a limited improvement of the O<sub>3</sub> simulation, due in part to the fact that the O<sub>3</sub> production in this region is NO<sub>x</sub> saturated in urban areas where most AQS monitors are deployed. Therefore, its effect is not as large as BCON or OI adjustments, which directly influence O<sub>3</sub> concentrations. A recent study by Jin et al. (2020) showed that the decrease in NO<sub>x</sub> emissions has shifted the NO<sub>x</sub>-saturated to NO<sub>x</sub>-sensitive regime transition zone closer to urban centers, approximately 40 to 60 km from the center (the highest emission point) of New York City. Therefore, it is expected that the effectiveness of emission adjustment will increase over time in this region. For surface NO<sub>2</sub>, the emission adjustment showed more significant impact on the simulated concentration. Considering both O<sub>3</sub> and NO<sub>2</sub> performance, the domain-average approach (EmisAdj\_avg) is selected for subsequent multi-adjustment simulations.



### 365 3.4 Effectiveness of combined adjustment methods

After assessing the effects of individual updates, we test how these updates can be combined to optimize forecasting performance. In the preceding sections, three groups of adjustment approaches have been included and evaluated. For each group, the best performing method has been identified, including the dynamic BCs, ICs with OI-bias, and rapid emission refresh (EmisAdj\_avg). With these selected updates, we design and conduct two multi-adjustment simulations, the first one used both the dynamic BCs and the OI-bias adjusted initial concentration files (BO for short) and the other one employed the NO<sub>x</sub> emission with projection from 2011 to 2018 together with the combination of BCON and OI-bias (BOE hereafter). Results of these combined adjustments are compared against the Control, BCON run and the NAQFC prediction.

First, we compare the predicted O<sub>3</sub> and NO<sub>2</sub> concentrations against in-situ observations in five subdomains and the overall domain with Taylor diagrams (Taylor, 2001) (Fig. 8). In this diagram, the relative skill of each forecasting system to reproduce the O<sub>3</sub> and NO<sub>2</sub> variability is represented using three statistical metrics: normalized standard deviation (SD), correlation (R), and centered root-mean-square difference (RMSD). Model skill is measured by the distance to the OBS point on these diagrams. The default (Control) run yielded a correlation coefficient of approximately 0.8 (0.77–0.84) in each subdomain while those with adjustments show stronger correlations with R all above 0.9. Furthermore, the performance in the OTHER areas is better than that in the five subdomains with the R value up to 0.97 and SD close to 1 (Fig. 7e). Taylor diagrams also reveal that these adjustments are even more effective over the low emission areas. The three adjusted runs (#2, 3, 4) have well reproduced surface O<sub>3</sub> concentrations over the NYC region. The simulations with BOE usually demonstrate a relatively lower O<sub>3</sub> concentration level than that with the BCON run or the combined BCON and OI run. This means in the overestimated areas (such as NYC, Fig. 8a), the simulations with emission adjustment show better performance than that without emission adjustment. In addition, these three simulations have similar biases and errors with NMB ranging from 4% to 22% and NME from 15 to 22% (Fig. 9a, 9c). These results illustrate the importance of combining complementary modeling system updates to reduce model uncertainties in a comprehensive way. A single update, such as emission adjustment, may result in a better emission input closer to the “true” level, but its effect can be offset by systematic biases caused by other inputs. Concurrent improvements of boundary conditions and initial concentrations allow a more realistic initial state for a demonstration of the effectiveness of the emission adjustment to improve O<sub>3</sub> forecasting (Fig. 9).

The Taylor diagrams show that the performance of variability of NO<sub>2</sub> predictions is generally worse than that of variability of O<sub>3</sub> predictions. Overlaid on the same diagrams, the points that represent NO<sub>2</sub> performance are all further away from the OBS point compared to that representing O<sub>3</sub> from the same simulations (Fig. 8). This is not surprising as O<sub>3</sub> has been one of the focal points in air quality modeling in the past decades, while NO<sub>2</sub> has not been scrutinized with the same intensity. All of the high-resolution simulations, including the Control run, perform better than the NAQFC run (Fig. 9), highlighting the benefit of using a high-resolution modeling system for predicting short-lived chemical species such as NO<sub>2</sub>. The NAQFC generally underestimates NO<sub>2</sub> concentrations in all subdomains. Since the boundary conditions used by the high-resolution CMAQ runs are derived from NAQFC, the large negative NO<sub>2</sub> bias from NAQFC also contributes to the overall bias to the high-resolution runs. The NO<sub>2</sub> bias is the smallest in the NYC subdomain and largest in its downwind New Haven-Hartford region. The correlation coefficient is between 0.8 and 0.9 in NYC, but lower than



0.6 in the New Haven-Hartford region (Fig. 8). Similarly, the NMB are within 10% in NYC but can be as large as -70% in the New Haven-Hartford region. Such a contrast suggests either an underestimate of emission sources in Connecticut, or flawed model chemistry and transport, or a combination of both.

#### 405 4. High O<sub>3</sub> episode simulations during the LISTOS field campaign

In this section, the newly developed high-resolution system, equipped with all forecast improvements (dynamic boundary conditions, optimal interpolation, and emission adjustment, or BOE), is used to simulate a high O<sub>3</sub> episode over the Long Island Sound region. During the high O<sub>3</sub> pollution event (August 28-29, 2018), surface O<sub>3</sub> concentrations exceeded the National Ambient Air Quality Standard (NAAQS) (daily maximum 8-hour average of 70 ppbv) at several  
410 monitoring locations, including one site (Colliers Mills) in New Jersey, one site (Riverhead) in New York, and five sites (Greenwich, Madison-Beach Road, Middletown-CVH-Shed, Stratford, and Westport) in Connecticut. While merely exceeding the threshold values by a few ppbv at most sites, the O<sub>3</sub> concentrations reached 84 ppbv at the Westport site, and 87 ppbv at the Stratford site. Considering the significant emission reduction and air quality improvements in the eastern United States (He et al., 2020; Qu et al., 2019), this episode, which occurred during a well-designed field campaign,  
415 offers a rare opportunity to assess how well a state-of-the-science air quality model can predict a high O<sub>3</sub> pollution event that is now less frequent than in the past decades.

##### 4.1 NO<sub>2</sub> prediction

CMAQ predictions of NO<sub>2</sub> surface concentrations and vertical column density are compared against ground and aircraft observations. NO<sub>2</sub> is not only a key precursor to tropospheric ozone, but also a proxy for traffic-related air pollution in  
420 many epidemiological studies (e.g., Jerrett et al., 2007). Within the LISTOS CMAQ domain, there are four active ground monitors with valid NO<sub>2</sub> readings during the study period. Hourly variations from AQS monitors, the BOE 3 km prediction, and the operational NAQFC prediction are illustrated in Fig. 10. Among these sites, the lowest NO<sub>2</sub> concentrations were observed at the Flax Pond site in the middle of Long Island, away from the major emission sources. Both BOE and NAQFC are able to reproduce the magnitude and diurnal variations of surface NO<sub>2</sub> concentrations at this  
425 site. The NO<sub>2</sub> concentration at the Queens College site, also located on Long Island though within NYC, is significantly higher than at the Flax Pond site, due to its close proximity to major sources such as the tunnels, harbors and highways. For this site, the BOE 3 km prediction is considerably better than that from the NAQFC prediction. Similarly, the BOE prediction outperforms the NAQFC at the New Haven site in Connecticut, where the surface NO<sub>2</sub> concentration reaches 40 ppbv on August 28 and 55 ppbv on August 29, 2018. The NAQFC predicted concentration is constantly below 10  
430 ppbv, severely underestimating the observations. In comparison, the BOE predicted concentration is much closer to the observations, although still underpredicting the latter. Finally, both models missed the first, primary peak on both days at the Westport, CT site, which is strongly influenced by the NY City plume and sea breeze circulation.

Next, the two model simulations are compared against the NO<sub>2</sub> VCD measured by NASA GCAS during the LISTOS field campaign. In order to allow a comparison between simulations and measurements from GCAS, the CMAQ  
435 prediction of NO<sub>2</sub> mixing ratio is vertically integrated from the surface to the layer which is the closest to the plane altitude to generate vertical column density (unit: molecules cm<sup>-2</sup>), GCAS data are averaged over the 3 km grid to provide a



spatially representative observation for the BOE simulation and over the 12km grid for the NAQFC simulation. We also sample the model data to match the actual measurement time. The GCAS observations show higher NO<sub>2</sub> VCD in the morning and lower values in the afternoon. This temporal pattern is well captured by both simulations. The GCAS observations depict an NO<sub>2</sub> hotspot over lower Manhattan, which is reproduced by both BOE and NAQFC simulations (Fig. 11). The observed and simulated VCDs are generally at the same magnitude ( $4\text{--}40\times 10^{15}$  molecules cm<sup>-2</sup>), with BOE better capturing the peak values. Both simulations, however, are biased high, outside the hotspot area, especially in the morning. The BOE prediction shows a larger area of high NO<sub>2</sub> VCD than that from GCAS, suggesting either a positive bias in NO<sub>x</sub> emissions or inefficient transformation and removal of emitted NO<sub>x</sub> in the CMAQ model. The high NO<sub>2</sub> VCD from the NAQFC simulation is lower than the measurements over lower Manhattan, and the high NO<sub>2</sub> VCD extends to an area larger than that from both GCAS and BOE. The performance is relatively unsatisfactory during the high polluting period on August 28 morning (Fig. 11e, 11i) with a correlation of only 0.56 for BOE and 0.44 for NAQFC. These low correlations could be partly caused by the high spatial variability of fine resolution measured VCD, so that the averaged VCD is still more variable than either model. In contrast, the spatial patterns of NO<sub>2</sub> VCD in the afternoon are better reproduced than in the morning (Table S2). And besides the uncertainties in the model, an evaluation conducted by Judd et al. (2019) showed that the absolute difference in GCAS from Pandora measurement has an average and standard deviation of  $-0.2\times 10^{15}\pm 2\times 10^{15}$  molecules cm<sup>-2</sup> and a percent difference on average of  $-1.5\%\pm 20\%$ , which indicates biases exist in GCAS retrievals. Overall, the BOE simulation at 3 km resolution is able to reproduce the observed NO<sub>2</sub> VCD with a higher correlation (0.74), a lower NMB (40%) and a lower NME (61%) than the NAQFC at 12 km resolution (0.57, 45% and 76%, respectively).

#### 4.2 O<sub>3</sub> prediction

One key result expected from the improved prediction system is to better reproduce high O<sub>3</sub> episodes, especially those events that cause the exceedance of NAAQS. Here we compare the model performance between BOE and NAQFC at the seven sites where the O<sub>3</sub> concentrations exceeded the NAAQS. Compared to NAQFC, BOE demonstrates enhanced prediction skill at all sites (Fig. 12). The results show that BOE can better capture peak O<sub>3</sub> values than NAQFC in the afternoon, a highly desired feature in predicting O<sub>3</sub> exceedances. Hourly surface O<sub>3</sub> concentrations reached more than 100 ppbv at four Connecticut sites, including Greenwich, Westport, Middletown-CVH-Shed, and Stratford. While neither BOE nor NAQFC is able to predict such high values, BOE reduces the bias by 10–20 ppbv during peak hours at these sites. The improvement of peak O<sub>3</sub> prediction is less significant on the other sites with lower observed O<sub>3</sub> concentration, but BOE still displays better performance than NAQFC. It is also interesting to observe that, regardless of its capability to predicting higher peaks, BOE does not cause an increase of false alarms. There are only three sites at which one or both simulations overpredict peak O<sub>3</sub> on the August 29, 2018. Compared to NAQFC, BOE shows larger over-prediction of the peak O<sub>3</sub> at the Greenwich site, but smaller overprediction at two other sites (Middletown and Westport).

Besides better peak prediction, BOE has also improved the prediction of the timing of peak O<sub>3</sub>. The peaks predicted by BOE are two to three hours earlier than that by NAQFC, which agree better with the timing of the observed peaks (Fig. 12). The BOE peaks are narrower than the NAQFC ones, so that the former follows the observed O<sub>3</sub> downslope and avoids the positive biases during late afternoon and early evening. Finally, BOE has improved the prediction of low O<sub>3</sub>



concentrations and nighttime O<sub>3</sub> valleys that are lower than those from NAQFC. Both simulations, however, are unable to reproduce the extreme low nighttime values at several sites. Overall, the BOE simulation performs better in capturing the daytime O<sub>3</sub> peaks and nighttime valleys, as well as the timing of both, with a mean correlation coefficient of 0.93 compared to 0.88 for the NAQFC simulation.

Vertical profiles of O<sub>3</sub> are compared between Langley Mobile O<sub>3</sub> Lidar (LMOL) observations and CMAQ simulations at the Westport site. As shown in Fig. 13, LMOL observations reveal that the O<sub>3</sub> concentration in the planetary boundary layer starts to build around 16:00–17:00 UTC and high concentrations (>70 ppbv), which extend to a height of about 1.5 km, last until 23:00 UTC on August 28 and 29. This pattern is reproduced by both the BOE and NAQFC simulations. Above the PBL, the variations of O<sub>3</sub> concentrations are also captured by both simulations. O<sub>3</sub> concentrations in the free troposphere are more controlled by regional O<sub>3</sub> production and transport than in the PBL. Consequently, the structure and magnitude of O<sub>3</sub> profiles are very similar between the BOE and NAQFC simulations, since the BOE simulation is driven by the dynamic boundary conditions derived from the same NAQFC simulation. Compared to that from the LMOL observations, the predicted O<sub>3</sub> concentrations from both simulations are biased low (high) above (below) 800 hPa. Between the two model simulations, the BOE run produces higher O<sub>3</sub> mixing ratio in the PBL. It also shows a better match with LMOL in the temporal variations of O<sub>3</sub> peaks, with a short-lived peak between 20:00–22:00 UTC on August 28, and persistent high O<sub>3</sub> plateaus between 16:00–23:00 UTC on August 29 (Fig. 13). The PBL in the BOE simulation extends well above 850 mbar, while the observed high O<sub>3</sub> from LMOL generally stays beneath this height, suggesting possible overprediction of the PBL height.

In general, the 3 km BOE simulation performs better to capture the temporal variability of the PBL and O<sub>3</sub> production but tends to overestimate both during the episode. In contrast, the NAQFC simulation has produced less pronounced temporal variations in both O<sub>3</sub> concentrations and PBL height in the lower troposphere, in particular on August 28 when this region experienced the worst air quality in several states. The NAQFC simulation, however, performed better during the time with lower O<sub>3</sub> concentrations, which resulted in an overall lower NMB (9%) and NME (21%) comparing to that in BOE (22% and 26% respectively). The BOE simulation, however, presented a much better reproduction of the O<sub>3</sub> variability in terms of correlation (0.71) than the NAQFC run (0.54). This suggests that the new 3 km BOE system is more responsive to the controlling factors that shape O<sub>3</sub> pollution, although the system needs to be further refined to reduce bias.

## 5. Summary

Improvement of air quality in the past decade renders the prediction of high ozone events more challenging. This study investigates the feasibility of designing a high-resolution air quality prediction system to capture these less frequent events with more accuracy. Relying on the observations collected during the Long Island Sound Tropospheric Ozone Study field campaign, we have assessed the effectiveness of various improvements to the predictions system to enhance the predictability of high O<sub>3</sub> episodes. These updates were then combined to explore how to further improve the predictability of both ozone and nitrogen dioxide. Finally, the modeling system with combined updates has been utilized to reproduce a severe high O<sub>3</sub> pollution event in the Long Island Sound and surrounding areas.



Different prediction system updates demonstrate varying potentials to improve O<sub>3</sub> and NO<sub>2</sub> prediction performance. For O<sub>3</sub> prediction, the most significant improvement comes from the dynamic boundary conditions derived from NOAA National Air Quality Forecast Capability (NAQFC), compared to that with the static boundary conditions. This is due in part to the fact that O<sub>3</sub> is a regional air pollutant and the relatively small model domain used in this study, making the O<sub>3</sub> prediction more susceptible to the influence of regional transport. Dynamic boundary conditions (BCs) are less influential for NO<sub>2</sub> prediction, for which all high-resolution simulations outperform the 12 km NAQFC simulation, highlighting the importance of spatially resolved emission and meteorology for the prediction of short-lived pollutants. The impact of improved initial concentrations through optimal interpolation (OI) is shown to be large in urban areas initially. The influence of OI adjustment, however, lingers for a longer period in an area with low emission density where emissions and chemical reactions make a smaller contribution to the O<sub>3</sub> budget than that in the area with high emission density. Finally, emission adjustment, which changes baseline emissions using the temporal trends derived from ground and satellite observations, only yields moderate improvement in O<sub>3</sub> prediction compared to that without emission adjustment. One possible direction to explore is to use atmospheric observations to constrain emissions through coupled data assimilation approaches in future efforts.

While the effectiveness of each update varies, a combination of these updates proves to outperform each single update. The new prediction system at 3 km resolution, equipped with dynamic BCs, OI and Emission adjustment (BOE), was used to simulate a high O<sub>3</sub> episode over the Long Island Sound region. Compared to 12 km resolution operational NAQFC, BOE is able to significantly reduce the biases in surface O<sub>3</sub> and NO<sub>2</sub> prediction. The BOE is also able to reproduce NO<sub>2</sub> vertical column density (VCD) by NASA Langley GCAS with higher accuracy than the NAQFC. More importantly, the BOE simulation shows considerable improvement in capturing the O<sub>3</sub> peaks and valleys, as well as the timing of both, with a correlation coefficient of 0.93 compared to that of NAQFC (0.88). Although limited to only one episode over the Long Island Sound, this study demonstrates feasible measures to improve the capability of air quality prediction systems to capture high O<sub>3</sub> episodes in a cleaner urban environment.

*Data Availability.* CMAQ and SMOKE model documentation and released versions of the source code are available on the US EPA modeling site <https://www.cmascenter.org/> (last access: December 2020). WRF is an open-source community model. The source code is available at [http://www2.mmm.ucar.edu/wrf/users/download/get\\_source.html](http://www2.mmm.ucar.edu/wrf/users/download/get_source.html) (last access: Nov 2020).

*Author Contribution.* DT and SM designed the study, conducted the simulations and wrote the manuscript. JW, XZ and PL helped development of the modeling system. LL, RS and LJ provided OMI and LISTOS field campaign data and helped interpreting the results. YT and TC provided code for the original OI method. All authors edited and commented on the manuscript. All authors read, revised, and approved the final paper.

*Competing interests.* The authors declare that they have no conflict of interest.



545 *Acknowledgement.* This work was partially supported by a National Research Council fellowship to S. Ma at NOAA Air Resources Laboratory and by NOAA Weather Program Office to D. Tong. The authors are grateful to the EPA and NYDEC for sharing the AQS data and to NASA for providing the OMI, GCAS and Langley Mobile O<sub>3</sub> Lidar datasets.

## References

- 550 Adhikary, B., Kulkarni, S., Dallura, A., Tang, Y., Chai, T., Leung, L. R., Qian, Y., Chung, C. E., Ramanathan, V. and Carmichael, G. R.: A regional scale chemical transport modeling of Asian aerosols with data assimilation of AOD observations using optimal interpolation technique, *Atmos. Environ.*, 42(37), 8600–8615, <https://doi.org/10.1016/j.atmosenv.2008.08.031>, 2008.
- Baker, K. R., Liljegren, J., Valin, L., Judd, L. M., Henderson, B. H., Szykman, J., Al-Saadi, J. A., Janz, S. J., Sareen, N. and Possiel, N.: Model-Measurement Comparison of Ozone and Precursors Along Land-Water Interfaces during the 2017 LMOS and 2018 LISTOS Field Campaigns, AGUFM, 2019, A21E-06, 2019.
- Berkoff, T., Gronoff, G., Baker, B., Lee, P., Dreessen, J. and Sullivan, J.: Comparison of tropospheric ozone vertical profiles between NASA ozone lidars and NOAA’s National Air Quality Forecasting Capability (NAQFC) model, AGUFM, 2019, A21E-02, <https://doi.org/10.1016/j.atmosenv.2010.04.044>, 2019.
- 560 Borge, R., López, J., Lumbreras, J., Narros, A. and Rodríguez, E.: Influence of boundary conditions on CMAQ simulations over the Iberian Peninsula, *Atmos. Environ.*, 44(23), 2681–2695, <https://doi.org/10.1016/j.atmosenv.2010.04.044>, 2010.
- Brunekreef, B. and Holgate, S. T.: Air pollution and health, *Lancet*, 360(9341), 1233–1242, [https://doi.org/10.1016/S0140-6736\(02\)11274-8](https://doi.org/10.1016/S0140-6736(02)11274-8), 2002.
- 565 Byun, D. and Schere, K. L.: Review of the governing equations, computational algorithms, and other components of the Models-3 Community Multiscale Air Quality (CMAQ) modeling system, <https://doi.org/10.1115/1.2128636>, 2006.
- Candiani, G., Carnevale, C., Finzi, G., Pisoni, E. and Volta, M.: A comparison of reanalysis techniques: Applying optimal interpolation and Ensemble Kalman Filtering to improve air quality monitoring at mesoscale, *Sci. Total Environ.*, 458, 7–14, <https://doi.org/10.1016/j.scitotenv.2013.03.089>, 2013.
- 570 Chai, T., Kim, H., Pan, L., Lee, P. and Tong, D.: Impact of Moderate Resolution Imaging Spectroradiometer aerosol optical depth and AirNow PM<sub>2.5</sub> assimilation on Community Multi-scale Air Quality aerosol predictions over the contiguous United States, *J. Geophys. Res. Atmos.*, 122(10), 5399–5415, <https://doi.org/10.1002/2016JD026295>, 2017.
- Chameides, W. L., Fehsenfeld, F., Rodgers, M. O., Cardelino, C., Martinez, J., Parrish, D., Lonneman, W., Lawson, D. R., Rasmussen, R. A. and Zimmerman, P.: Ozone precursor relationships in the ambient atmosphere, *J. Geophys. Res. Atmos.*, 97(D5), 6037–6055, 1992.
- 575 De Young, R., Carrion, W., Ganoë, R., Pliutau, D., Gronoff, G., Berkoff, T. and Kuang, S.: Langley mobile ozone lidar: ozone and aerosol atmospheric profiling for air quality research, *Appl. Opt.*, 56(3), 721–730, <https://doi.org/10.1364/AO.56.000721>, 2017.



- 580 Dix, B., de Bruin, J., Roosenbrand, E., Vlemmix, T., Francoeur, C., Gorchov-Negron, A., McDonald, B., Zhizhin, M.,  
Elvidge, C. and Veefkind, P.: Nitrogen Oxide Emissions from US Oil and Gas Production: Recent Trends and Source  
Attribution, *Geophys. Res. Lett.*, 47(1), e2019GL085866, <https://doi.org/10.1029/2019GL085866>, 2020.
- Dunlea, E. J., Herndon, S. C., Nelson, D. D., Volkamer, R. M., San Martini, F., Sheehy, P. M., Zahniser, M. S., Shorter,  
J. H., Wormhoudt, J. C. and Lamb, B. K.: Evaluation of nitrogen dioxide chemiluminescence monitors in a polluted  
585 urban environment, <https://doi.org/10.5194/acp-7-2691-2007>, 2007.
- Feng, J., Chan, E., and Vet, R.: Air quality in the eastern United States and Eastern Canada for 1990–2015: 25 years of  
change in response to emission reductions of SO<sub>2</sub> and NO<sub>x</sub> in the region, *Atmos. Chem. Phys.*, 20, 3107–3134,  
<https://doi.org/10.5194/acp-20-3107-2020>, 2020.
- Gantt, B., Kelly, J. T. and Bash, J. O.: Updating sea spray aerosol emissions in the Community Multiscale Air Quality  
590 (CMAQ) model version 5.0. 2., *Geosci. Model Dev. Discuss.*, 8(5), <https://doi.org/10.5194/gmd-8-3733-2015>, 2015.
- Gong, S. L.: A parameterization of sea-salt aerosol source function for sub-and super-micron particles, *Global  
Biogeochem. Cycles*, 17(4), <https://doi.org/10.1029/2003GB002079>, 2003.
- Gronoff, G., Robinson, J., Berkoff, T., Swap, R., Farris, B., Schroeder, J., Halliday, H. S., Knepp, T., Spinei, E. and  
Carrion, W.: A method for quantifying near range point source induced O<sub>3</sub> titration events using Co-located Lidar and  
595 Pandora measurements, *Atmos. Environ.*, 204, 43–52, <https://doi.org/10.1016/j.atmosenv.2019.01.052>, 2019.
- He, H., Liang, X.-Z., Sun, C., Tao, Z. and Tong, D. Q.: The long-term trend and production sensitivity change in the US  
ozone pollution from observations and model simulations., *Atmos. Chem. Phys.*, 20(5), <https://doi.org/10.5194/acp-20-3191-2020>, 2020.
- Henderson, B. H., Akhtar, F., Pye, H. O. T., Napelenok, S. L. and Hutzell, W. T.: A database and tool for boundary  
600 conditions for regional air quality modeling: description and evaluation, *Geosci. Model Dev.*, 7(1), 339–360,  
<https://doi.org/10.5194/gmd-7-339-2014>, 2014.
- Héroux, M.-E., Anderson, H. R., Atkinson, R., Brunekreef, B., Cohen, A., Forastiere, F., Hurley, F., Katsouyanni, K.,  
Krewski, D. and Krzyzanowski, M.: Quantifying the health impacts of ambient air pollutants: recommendations of a  
WHO/Europe project, *Int. J. Public Health*, 60(5), 619–627, <https://doi.org/10.1007/s00038-015-0690-y>, 2015.
- 605 Hogrefe, C., Hao, W., Civerolo, K., Ku, J.-Y., Sistla, G., Gaza, R. S., Sedefian, L., Schere, K., Gilliland, A. and Mathur,  
R.: Daily simulation of ozone and fine particulates over New York State: findings and challenges, *J. Appl. Meteorol.  
Climatol.*, 46(7), 961–979, 2007.
- Hogrefe, C., Hao, W., Zalewsky, E., Ku, J., Lynn, B., Rosenzweig, C., Schultz, M. G., Rast, S., Newchurch, M. J. and  
Wang, L.: An analysis of long-term regional-scale ozone simulations over the Northeastern United States: variability  
610 and trends, *Atmos. Chem. Phys.*, 11(2), 23045–23090, doi:10.5194/acp-11-567-2011, <https://doi.org/10.5194/acp-11-567-2011>, 2010.
- Houyoux, M., Vukovich, J., Brandmeyer, J. E., Seppanen, C. and Holland, A.: Sparse matrix operator kernel emissions  
modeling system-SMOKE User manual, Prep. by MCNC-North Carolina Supercomputing Center, Environ. Programs,  
Res. Triangle Park. NC, 2000.



- 615 Jerrett, M., Arain, M. A., Kanaroglou, P., Beckerman, B., Crouse, D., Gilbert, N. L., Brook, J. R., Finkelstein, N. and Finkelstein, M. M.: Modeling the intraurban variability of ambient traffic pollution in Toronto, Canada, *J. Toxicol. Environ. Heal. Part A*, 70(3–4), 200–212, <https://doi.org/10.1080/15287390600883018>, 2007.
- Jin, X., Fiore, A., Boersma, K. F., Smedt, I. D. and Valin, L., Inferring Changes in Summertime Surface Ozone–NO<sub>x</sub>–VOC Chemistry over US Urban Areas from Two Decades of Satellite and Ground-Based Observations. *Environ. Sci. Technol.*, 54(11), 6518–6529, <https://doi.org/10.1021/acs.est.9b07785>, 2020.
- 620 Judd, L. M., Al-Saadi, J. A., Janz, S. J., Kowalewski, M. G., Pierce, R. B., Szykman, J. J., Valin, L. C., Swap, R., Cede, A., Mueller, M., Tiefengraber, M., Abuhassan, N., and Williams, D.: Evaluating the impact of spatial resolution on tropospheric NO<sub>2</sub> column comparisons within urban areas using high-resolution airborne data, *Atmos. Meas. Tech.*, 12, 6091–6111, <https://doi.org/10.5194/amt-12-6091-2019>, 2019.
- 625 Kim, J. Y., Burnett, R. T., Neas, L., Thurston, G. D., Schwartz, J., Tolbert, P. E., Brunekreef, B., Goldberg, M. S. and Romieu, I.: Panel discussion review: session two—interpretation of observed associations between multiple ambient air pollutants and health effects in epidemiologic analyses, *J. Expo. Sci. Environ. Epidemiol.*, 17(2), S83–S89, Panel discussion review: session two—interpretation of observed associations between multiple ambient air pollutants and health effects in epidemiologic analyses, 2007.
- 630 Kowalewski, M. G. and Janz, S. J.: Remote sensing capabilities of the GeoCAPE Airborne Simulator, in *Earth Observing Systems XIX*, vol. 9218, p. 92181I, International Society for Optics and Photonics., <https://doi.org/10.1117/12.2062058>, 2014.
- Krotkov, N. A., McLinden, C. A., Li, C., Lamsal, L. N., Celarier, E. A., Marchenko, S. V, Swartz, W. H., Bucsela, E. J., Joiner, J. and Duncan, B. N.: Aura OMI observations of regional SO<sub>2</sub> and NO<sub>2</sub> pollution changes from 2005 to 2015, *Atmos. Chem. Phys.*, 16(7), 4605, 2016.
- 635 Khan, A.W., Kumar, P., Impact of chemical initial and lateral boundary conditions on air quality prediction. *Adv. Sp. Res.* 64, 1331–1342, <https://doi.org/10.1016/j.asr.2019.06.028>, 2019.
- Lamsal, L. N., Krotkov, N. A., Vasilkov, A., Marchenko, S., Qin, W., Yang, E.-S., Fasnacht, Z., Joiner, J., Choi, S., Haffner, D., Swartz, W. H., Fisher, B., and Bucsela, E.: OMI/Aura Nitrogen Dioxide Standard Product with Improved Surface and Cloud Treatments, *Atmos. Meas. Tech. Discuss.*, <https://doi.org/10.5194/amt-2020-200>, in review, 2020.
- 640 Lee, P., McQueen, J., Stajner, I., Huang, J., Pan, L., Tong, D., Kim, H., Tang, Y., Kondragunta, S. and Ruminski, M.: NAQFC developmental forecast guidance for fine particulate matter (PM<sub>2.5</sub>), *Weather Forecast.*, 32(1), 343–360, <https://doi.org/10.1175/WAF-D-15-0163.1>, 2017.
- Lee, S.-H., Kim, S.-W., Trainer, M., Frost, G. J., McKeen, S. A., Cooper, O. R., Flocke, F., Holloway, J. S., Neuman, J. A. and Ryerson, T.: Modeling ozone plumes observed downwind of New York City over the North Atlantic Ocean during the ICARTT field campaign., *Atmos. Chem. Phys. Discuss.*, 11(5), <https://doi.org/10.5194/acp-11-7375-2011>, 2011.
- 645 Levelt, P. F., van den Oord, G. H. J., Dobber, M. R., Malkki, A., Visser, H., de Vries, J., Stammes, P., Lundell, J. O. V and Saari, H.: The ozone monitoring instrument, *IEEE Trans. Geosci. Remote Sens.*, 44(5), 1093–1101, <https://doi.org/10.1109/TGRS.2006.872333>, 2006.
- 650



- Liu, T.-H., Jeng, F.-T., Huang, H.-C., Berge, E. and Chang, J. S.: Influences of initial conditions and boundary conditions on regional and urban scale Eulerian air quality transport model simulations, *Chemosphere-Global Chang. Sci.*, 3(2), 175–183, [https://doi.org/10.1016/S1465-9972\(00\)00048-9](https://doi.org/10.1016/S1465-9972(00)00048-9), 2001.
- 655 Long, R., Hall, E., Beaver, M., Duvall, R., Kaushik, S., Kronmiller, K., Wheeler, M., Garvey, S., Drake, Z. and McElroy, F.: Performance of the Proposed New Federal Reference Methods for Measuring Ozone Concentrations in Ambient Air. US Environmental Protection Agency. Washington, DC, EPA/600/R-14/432 (NTIS PB2015e101240), 2014.
- Luecken, D. J., Yarwood, G. and Hutzell, W. T.: Multipollutant modeling of ozone, reactive nitrogen and HAPs across the continental US with CMAQ-CB6, *Atmos. Environ.*, 201, 62–72, <https://doi.org/10.1016/j.atmosenv.2018.11.060>, 2019.
- 660 Makar, P. A., Gong, W., Mooney, C., Zhang, J., Davignon, D., Samaali, M., Moran, M. D., He, H., Tarasick, D. W. and Sills, D.: Dynamic adjustment of climatological ozone boundary conditions for air-quality forecasts, *Atmos. Chem. Phys. Discuss.*, 10(6), 13643–13688, <https://doi.org/10.5194/acp-10-8997-2010>, 2010.
- McClenny, W. A., Williams, E. J., Cohen, R. C. and Stutz, J.: Preparing to measure the effects of the NOX SIP Call—methods for ambient air monitoring of NO, NO<sub>2</sub>, NO<sub>y</sub>, and individual NO<sub>x</sub> species, *J. Air Waste Manage. Assoc.*, 665 52(5), 542–562, <https://doi.org/10.1080/10473289.2002.10470801>, 2002.
- National Research Council: Rethinking the ozone problem in urban and regional air pollution, National Academies Press., 1992.
- Nowlan, C. R., Liu, X., Janz, S. J., Kowalewski, M. G., Chance, K., Follette-Cook, M. B., Fried, A., Abad, G. G., Herman, J. R. and Judd, L. M.: Nitrogen dioxide and formaldehyde measurements from the GEOstationary Coastal and Air 670 Pollution Events (GEO-CAPE) airborne simulator over Houston, Texas, <https://doi.org/10.5194/amt-2018-156>, 2018.
- Pan, L., Tong, D., Lee, P., Kim, H.-C. and Chai, T.: Assessment of NO<sub>x</sub> and O<sub>3</sub> forecasting performances in the US National Air Quality Forecasting Capability before and after the 2012 major emissions updates, *Atmos. Environ.*, 95, 610–619, <https://doi.org/10.1016/j.atmosenv.2014.06.020>, 2014.
- 675 Pierce, T., Geron, C., Bender, L., Dennis, R., Tonnesen, G. and Guenther, A.: Influence of increased isoprene emissions on regional ozone modeling, *J. Geophys. Res. Atmos.*, 103(D19), 25611–25629, 1998.
- Pour-Biazar, A., Khan, M., Wang, L., Park, Y., Newchurch, M., McNider, R. T., Liu, X., Byun, D. W. and Cameron, R.: Utilization of satellite observation of ozone and aerosols in providing initial and boundary condition for regional air quality studies, *J. Geophys. Res. Atmos.*, 116(D18), <https://doi.org/10.1029/2010JD015200>, 2011.
- 680 Qu, Z.; Henze, D.K.; Li, C.; Theys, N.; Wang, Y.; Wang, J.; Wang, W.; Han, J.; Shim, C.; Dickerson, R.R.; Ren, X., SO<sub>2</sub> Emission Estimates Using OMI SO<sub>2</sub> Retrievals for 2005-2017. , *Journal of Geophysical Research: Atmospheres*, Vol. 124, Issue 4, 8336-8359, <https://doi.org/10.1029/2019JD030243>, 2019.
- Sandu, A., Chai, T. and Carmichael, G. R.: Integration of Models and Observations—a Modern Paradigm for Air Quality Simulations, *Model. Pollut. Complex Environ. Syst.*, 2, 419, 2010.
- 685 Shepard, D., A two-dimensional interpolation function for irregularly-spaced data, in: Proceedings of the 1968 23rd ACM National Conference. 517–524, <https://doi.org/10.1145/800186.810616>, 1968.



- Shu, Q., Baker, K. R., Napelenok, S. L., Szykman, J., Valin, L. and Plessel, T.: Multi-scale Analysis of Ozone Source Apportionment Using CMAQ-ISAM during 2018 LISTOS Field Campaign, AGUFM, 2019, A31E-06, 2019.
- 690 Silvern, R. F., Jacob, D. J., Mickley, L. J., Sulprizio, M. P., Travis, K. R., Marais, E. A., Cohen, R. C., Laughner, J. L., Choi, S. and Joiner, J.: Using satellite observations of tropospheric NO<sub>2</sub> columns to infer long-term trends in US NO<sub>x</sub> emissions: the importance of accounting for the free tropospheric NO<sub>2</sub> background, *Atmos. Chem. Phys.*, 19(13), 8863–8878, <https://doi.org/10.5194/acp-19-8863-2019>, 2019.
- Simon, H., Reff, A., Wells, B., Xing, J. and Frank, N.: Ozone trends across the United States over a period of decreasing NO<sub>x</sub> and VOC emissions, *Environ. Sci. Technol.*, 49(1), 186–195, <https://doi.org/10.1021/es504514z>, 2015.
- 695 Skamarock, W. C., Klemp, J. B., Dudhia, J., Gill, D. O., Barker, D. M., Wang, W. and Powers, J. G.: A description of the advanced research WRF version 2, National Center For Atmospheric Research Boulder Co Mesoscale and Microscale, <https://doi.org/10.5065/1dfh-6p972005>.
- Spicer, C. W.: Smog chamber studies of nitrogen oxide (NO<sub>x</sub>) transformation rate and nitrate precursor relationships, *Environ. Sci. Technol.*, 17(2), 112–120, <https://doi.org/10.1021/es00108a010>, 1983.
- 700 Sullivan, J. T., Berkoff, T., Gronoff, G., Knepp, T., Pippin, M., Allen, D., Twigg, L., Swap, R., Tzortziou, M. and Thompson, A. M.: The Ozone Water–Land Environmental Transition Study, UMBC Fac. Collect., <https://doi.org/10.1175/BAMS-D-18-0025.1>, 2019.
- Tang, Y. H., Pagowski, M., Chai, T. F., Pan, L., Lee, P., Baker, B., Kumar, R., Delle Monache, L., Tong, D. and Kim, H.-C.: A case study of aerosol data assimilation with the Community Multi-scale Air Quality Model over the contiguous United States using 3D-Var and optimal interpolation methods, 2017.
- 705 Tang, Y., Carmichael, G. R., Thongboonchoo, N., Chai, T., Horowitz, L. W., Pierce, R. B., Al-Saadi, J. A., Pfister, G., Vukovich, J. M. and Avery, M. A.: Influence of lateral and top boundary conditions on regional air quality prediction: A multiscale study coupling regional and global chemical transport models, *J. Geophys. Res. Atmos.*, 112(D10), <https://doi.org/10.1029/2006JD007515>, 2007.
- 710 Tang, Y., Chai, T., Pan, L., Lee, P., Tong, D., Kim, H.-C. and Chen, W.: Using optimal interpolation to assimilate surface measurements and satellite AOD for ozone and PM<sub>2.5</sub>: A case study for July 2011, *J. Air Waste Manage. Assoc.*, 65(10), 1206–1216, <https://doi.org/10.1080/10962247.2015.1062439>, 2015.
- Tang, Y., Lee, P., Tsidulko, M., Huang, H.-C., McQueen, J. T., DiMego, G. J., Emmons, L. K., Pierce, R. B., Thompson, A. M. and Lin, H.-M.: The impact of chemical lateral boundary conditions on CMAQ predictions of tropospheric ozone over the continental United States, *Environ. fluid Mech.*, 9(1), 43–58, <https://doi.org/10.1007/s10652-008-9092-5>, 2009.
- 715 Tang, Y.H., Pagowski, M., Chai, T.F., Pan, L., Lee, P., Baker, B., Kumar, R., Delle Monache, L., Tong, D., Kim, H.-C., A case study of aerosol data assimilation with the Community Multi-scale Air Quality Model over the contiguous United States using 3D-Var and optimal interpolation methods, *Geosci. Model Dev.*, 10, 4743–4758, <https://doi.org/10.5194/gmd-10-4743-2017>, 2017.
- 720 Taylor, K. E.: Summarizing multiple aspects of model performance in a single diagram, *J. Geophys. Res. Atmos.*, 106(D7), 7183–7192, <https://doi.org/10.1029/2000JD900719>, 2001.



- Tong, D. and Y. Tang. Advancing Air Quality Forecasting to Protect Human Health. *Environmental Managers*, October 2018, Available online at: <https://pubs.awma.org/flip/EM-Oct-2018/tong.pdf>. (accessed on 11.13.20)
- 725 Tong, D. Q. and Mauzerall, D. L.: Spatial variability of summertime tropospheric ozone over the continental United States: Implications of an evaluation of the CMAQ model, *Atmos. Environ.*, 40(17), 3041–3056, 2006.
- Tong, D. Q., Dan, M., Wang, T. and Lee, P.: Long-term dust climatology in the western United States reconstructed from routine aerosol ground monitoring, *Atmos. Chem. Phys.*, 12(11), 5189–5205, <https://doi.org/10.5194/acp-12-5189-2012>, 2012.
- 730 Tong, D. Q., Lamsal, L., Pan, L., Ding, C., Kim, H., Lee, P., Chai, T., Pickering, K. E. and Stajner, I.: Long-term NO<sub>x</sub> trends over large cities in the United States during the great recession: Comparison of satellite retrievals, ground observations, and emission inventories, *Atmos. Environ.*, 107, 70–84, <https://doi.org/10.1016/j.atmosenv.2015.01.035>, 2015.
- 735 Tong, D., Pan, L., Chen, W., Lamsal, L., Lee, P., Tang, Y., Kim, H., Kondragunta, S. and Stajner, I.: Impact of the 2008 Global Recession on air quality over the United States: Implications for surface ozone levels from changes in NO<sub>x</sub> emissions, *Geophys. Res. Lett.*, 43(17), 9280–9288, <https://doi.org/10.1002/2016GL069885>, 2016.
- US EPA: The Green Book Nonattainment Areas for Criteria Pollutants. Available online at: <http://www.epa.gov/airquality/greenbook/index.html> (accessed on 11.13.20). 2020.
- 740 Wang, Y., Sartelet, K., Bocquet, M. and Chazette, P.: Assimilation of ground versus lidar observations for PM<sub>10</sub> forecasting, *Atmos. Chem. Phys.*, <https://doi.org/10.5194/acp-13-269-2013>, 2013.
- Wolff, G. T. and Liroy, P. J.: Development of an ozone river associated with synoptic scale episodes in the eastern United States, *Environ. Sci. Technol.*, 14(10), 1257–1260, <https://doi.org/10.1021/es60170a011>, 1980.
- Wu, L., Mallet, V., Bocquet, M. and Sportisse, B.: A comparison study of data assimilation algorithms for ozone forecasts, *J. Geophys. Res. Atmos.*, 113(D20), <https://doi.org/10.1029/2008JD009991>, 2008.
- 745 Zhou, W., Cohan, D. S. and Napelenok, S. L.: Reconciling NO<sub>x</sub> emissions reductions and ozone trends in the US, 2002–2006, *Atmos. Environ.*, 70, 236–244, <https://doi.org/10.1016/j.atmosenv.2012.12.038>, 2013.



## Tables and Figures

750 **Table 1. Model adjustment and simulation design for the 3 km forecasting system**

Name	Description
1 Control	Simulation with profile BCs, no adjustment
2 BCON	Same as Control, but BCs replaced with NAQFC prediction
3 OI (3 Cases)	Initial concentrations adjusted by three OI methods (OI_avg, OI_idw and OI_bias)
4 EmisAdj (2 Cases)	NO <sub>x</sub> emissions adjusted using observed trends from ground and satellite sensors (EmisAdj_whole, EmisAdj_sub)
5 Combined (2 Cases)	Combination of different techniques. BCON+OI, BCON+OI+EmisAdj

**Table 2: Regional mean statistical metrics between observed and simulated O<sub>3</sub> during the episode**

Stats\Runs	Control	OI_avg	OI_idw	OI_bias
CORR	0.81	0.84	0.85	0.85
RMSE	14.97	14.30	13.79	13.72
NMB	-30%	-29%	-27%	-27%
NME	34%	33%	31%	31%

CORR: correlation coefficient, RMSE: relative mean square error, NMB: normalized mean bias, NME: normalized mean error.

755 **Table 3: Same with Table 2 but for NO<sub>2</sub>**

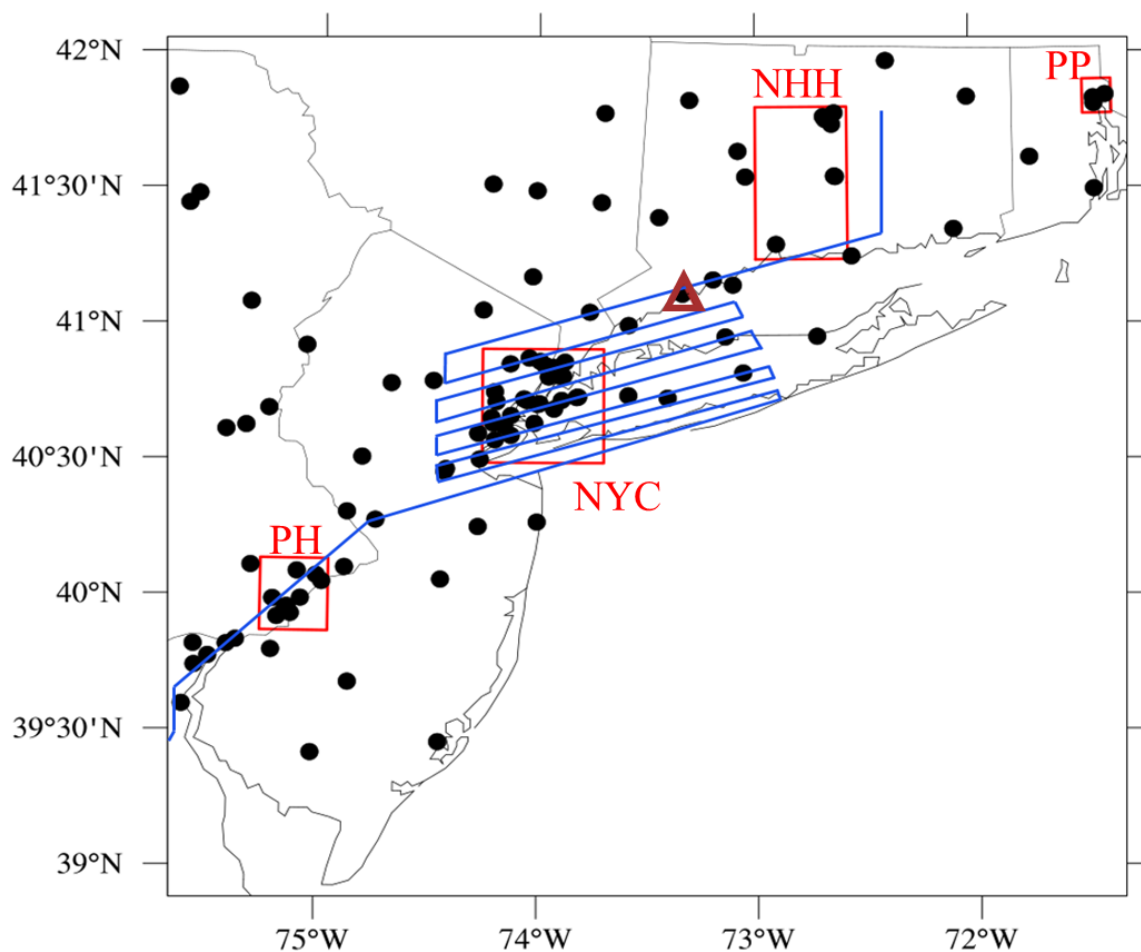
Stats\Runs	Control	OI_avg	OI_idw	OI_bias
CORR	0.69	0.69	0.69	0.70
RMSE	4.12	4.11	4.08	4.08
NMB	-17%	-17%	-15%	-17%
NME	35%	35%	35%	34%

**Table 4: Statistical metrics of O<sub>3</sub> and NO<sub>2</sub> simulations after NO<sub>x</sub> emission adjustment**

Stats\Runs	O <sub>3</sub>		NO <sub>2</sub>		
	EmisAdj_avg	EmisAdj_sub	Stats\Runs	EmisAdj_avg	EmisAdj_sub
CORR	0.81	0.81	CORR	0.69	0.69
RMSE	14.71	14.41	RMSE	4.62	4.96
NMB	-29%	-28%	NMB	-31%	-37%
NME	33%	32%	NME	38%	42%

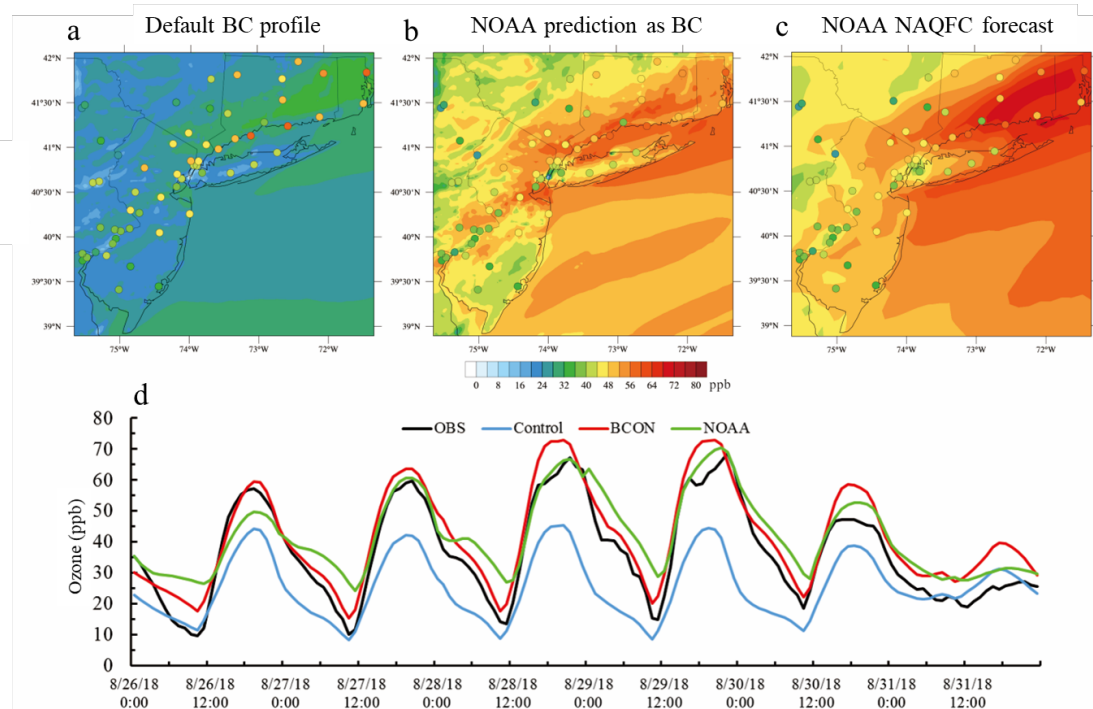


760



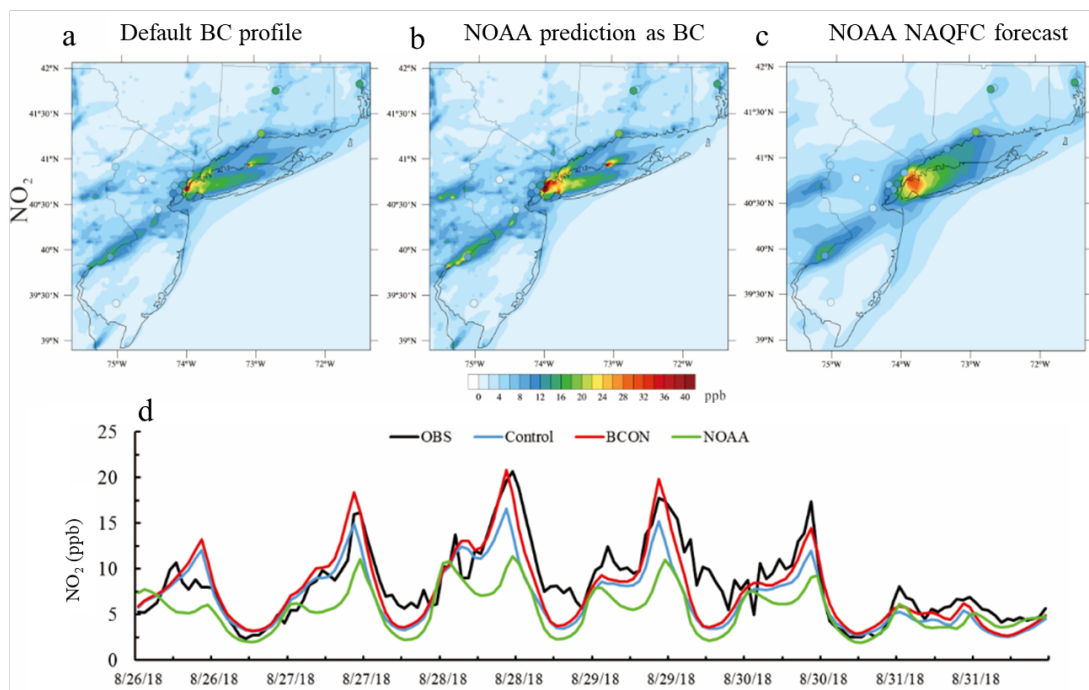
765 Figure 1: Study area over the Long Island Sound and surrounding areas. Red boxes depict four subdomains: New York City (NYC),  
Philadelphia (PH), New Haven-Hartford region (NHH), and Providence-Pawtucket region (PP). Black circles indicate the locations of  
EPA ground air quality monitors, the brown triangle indicates the TOLNet O<sub>3</sub> site located in Westport, CT, and the blue lines present  
an example flight path conducted by the NASA B200 aircraft on August 28–29, 2018.

770



775

Figure 2: Predicted O<sub>3</sub> concentrations from (a) Control, (b) BCON and (c) NOAA NAQFC simulations on August 29, 2018, and (d) comparison of domain-averaged hourly O<sub>3</sub> concentrations with EPA AirNow measurements during the episode. Colored circles at the top panels depict the observed concentrations from ground measurements.



780

Figure 3: Predicted NO<sub>2</sub> concentrations from (a) Control, (b) BCON and (c) NOAA NAQFC simulations on August 29, 2018, and (d) comparison of domain-averaged hourly NO<sub>2</sub> concentrations to EPA AirNow measurements during the episode. Colored circles at the top panels depict the observed concentrations from ground measurements.

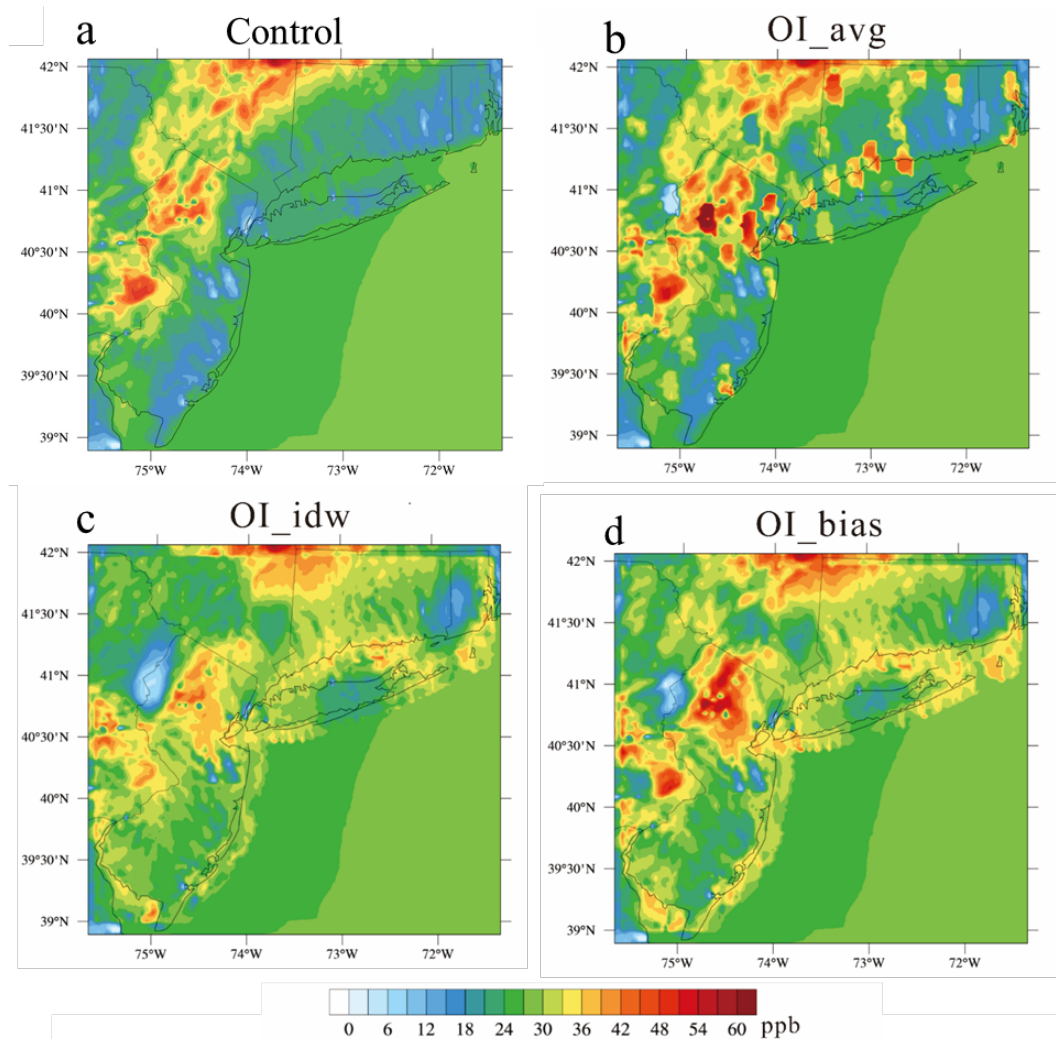
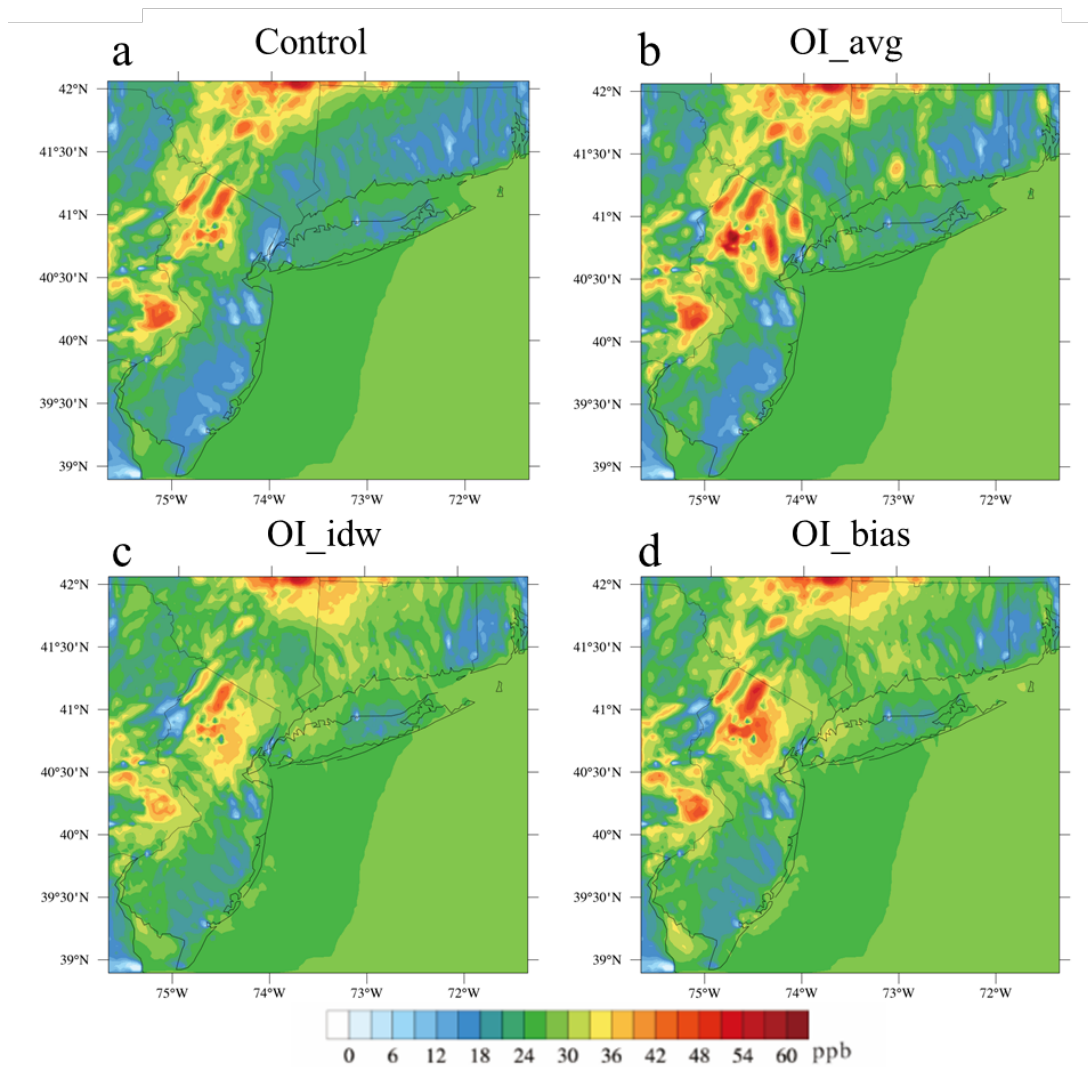


Figure 4: Initial concentration of surface O<sub>3</sub> on August 26 adjusted by OI\_avg, OI\_idw and OI\_bias.

785



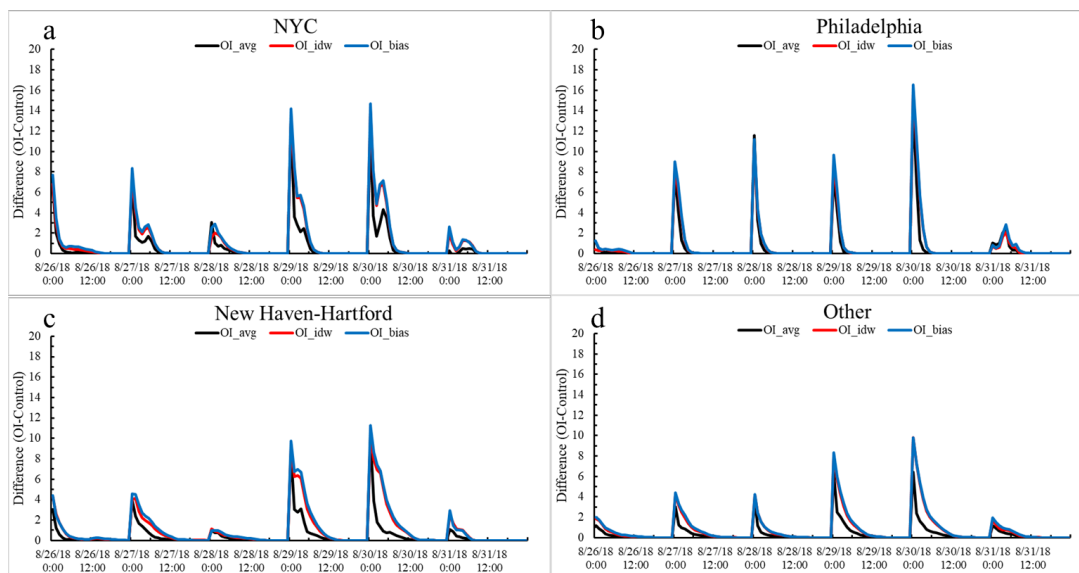


Figure 6. Effects of improved initial concentrations on hourly surface  $O_3$  in three metropolitan areas (New York, Philadelphia, and New Haven-Hartford) and the rest of domain using three Optimal Interpolation (OI) approaches (OI\_avg, OI\_idw, and OI\_bias).

795

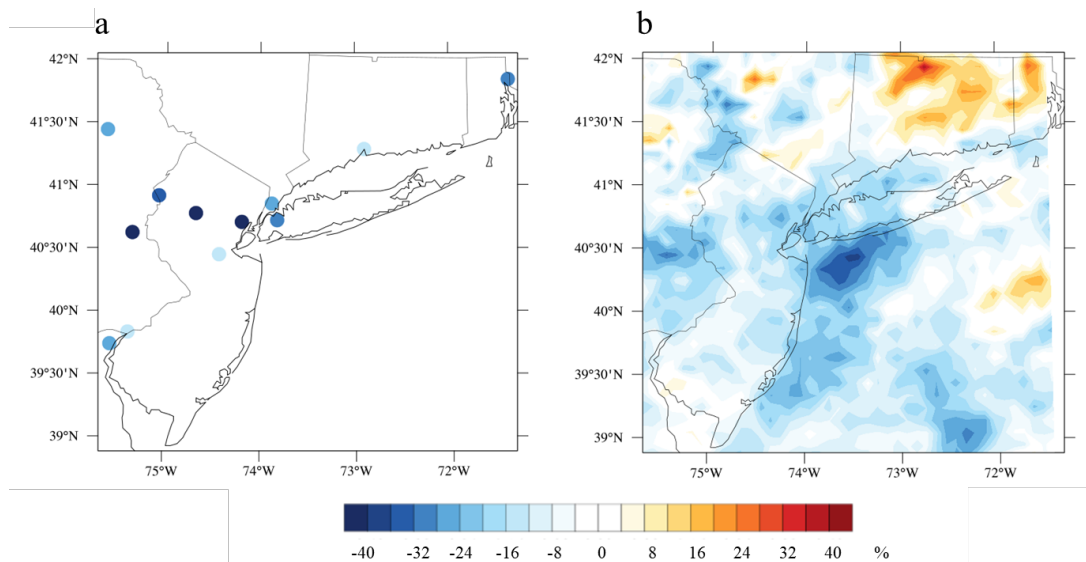
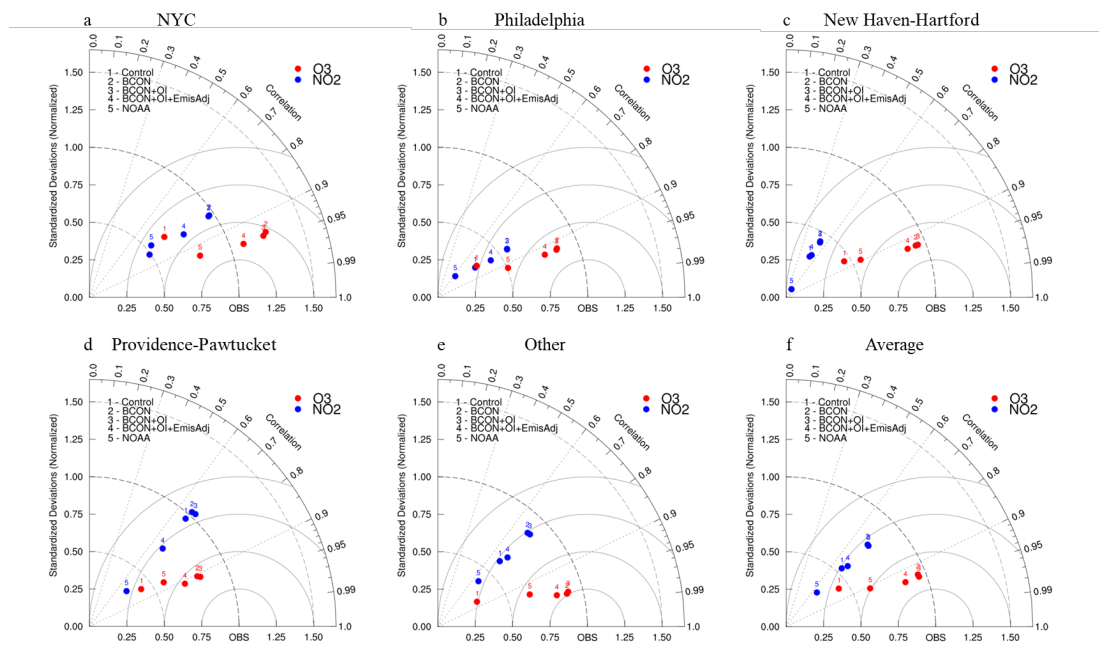


Figure 7: Differences in  $\text{NO}_x$  or  $\text{NO}_2$  observed by (a) AQS and (b) OMI from summer 2011 to summer 2018 over the model domain.



800 Figure 8: Model performance in Taylor diagrams of O<sub>3</sub> and NO<sub>2</sub> simulated by five runs, including the Control run, dynamic boundary conditions (BCON), boundary conditions with optimal interpolation (BCON+OI), and an all adjustment run including emission adjustment (BOE), and the operational NOAA national air quality forecast capability (NAQFC) run during the episode over five subdomains and the overall domain (Average).



805

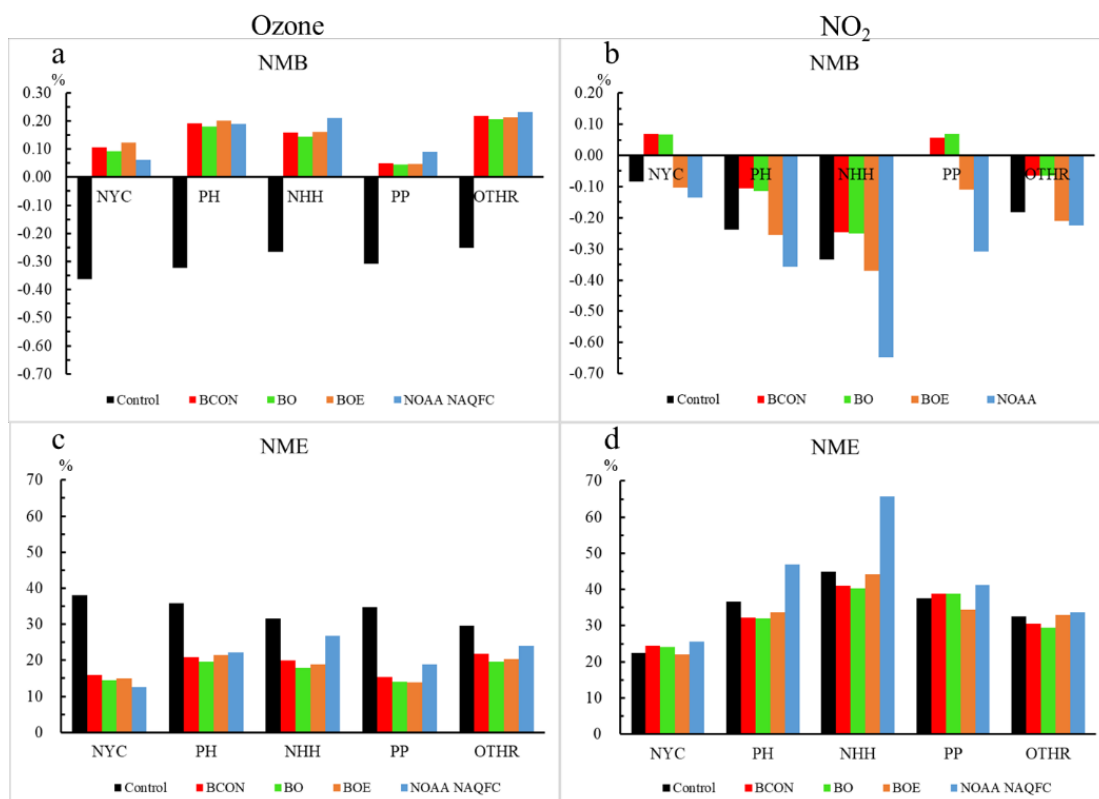
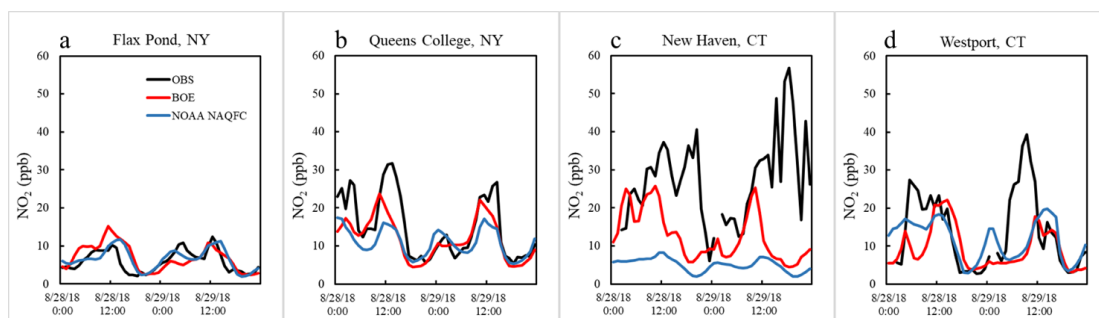
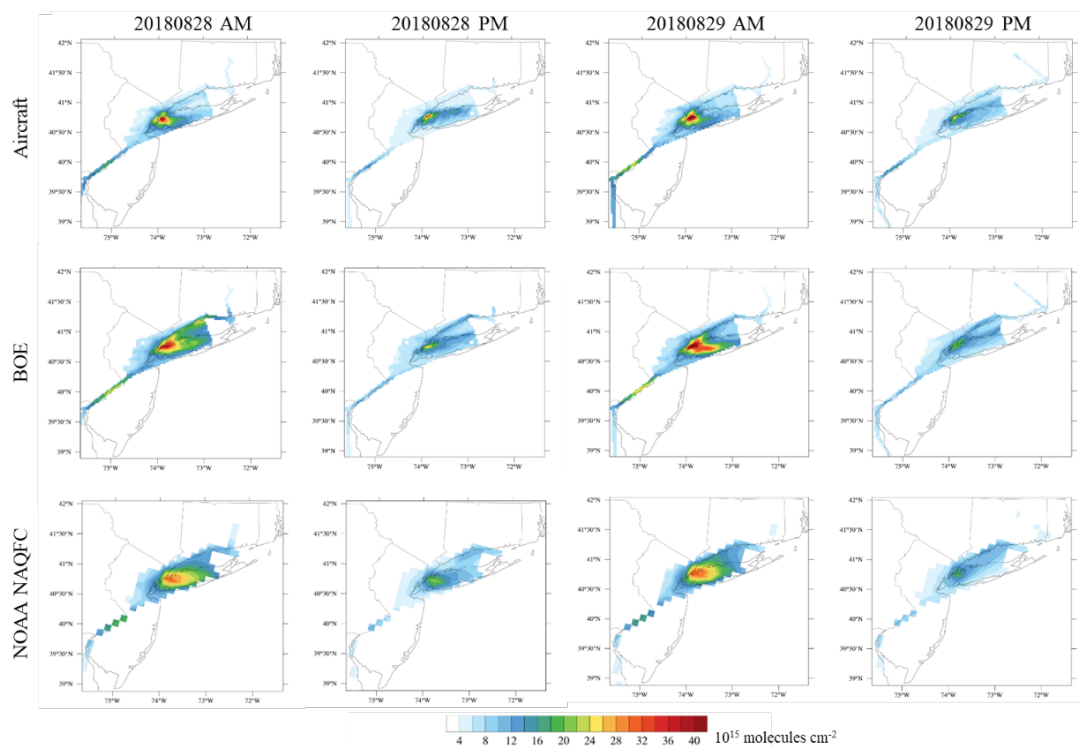


Figure 9: Comparisons of model performance for surface O<sub>3</sub> and NO<sub>2</sub> concentrations from five CMAQ simulations against measurements from the Air Quality System monitors. These simulations include the Control run, dynamic boundary conditions (BCON), boundary conditions with optimal interpolation (BCON+OI), and an all adjustment run including emission adjustment (BCOI+OI+EmisAdj), and the operational NOAA national air quality forecast capability (NAQFC) run during the episode over five subdomains. Two performance metrics are used here: normalized mean bias (NMB) and normalized mean error (NME).

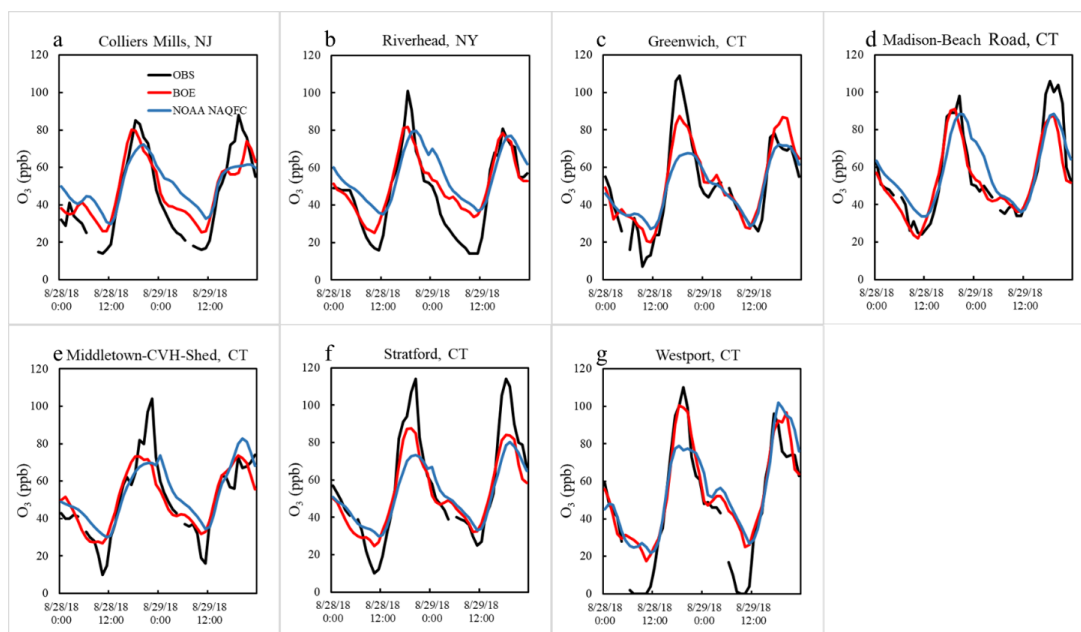
810



815 **Figure 10: Variations of observed and simulated surface NO<sub>2</sub> concentrations at (a) Flax Pond, NY; (b) Queens College, NY; (c) New Haven, CT; and (d) Westport, CT sites during August 28–29, 2018.**

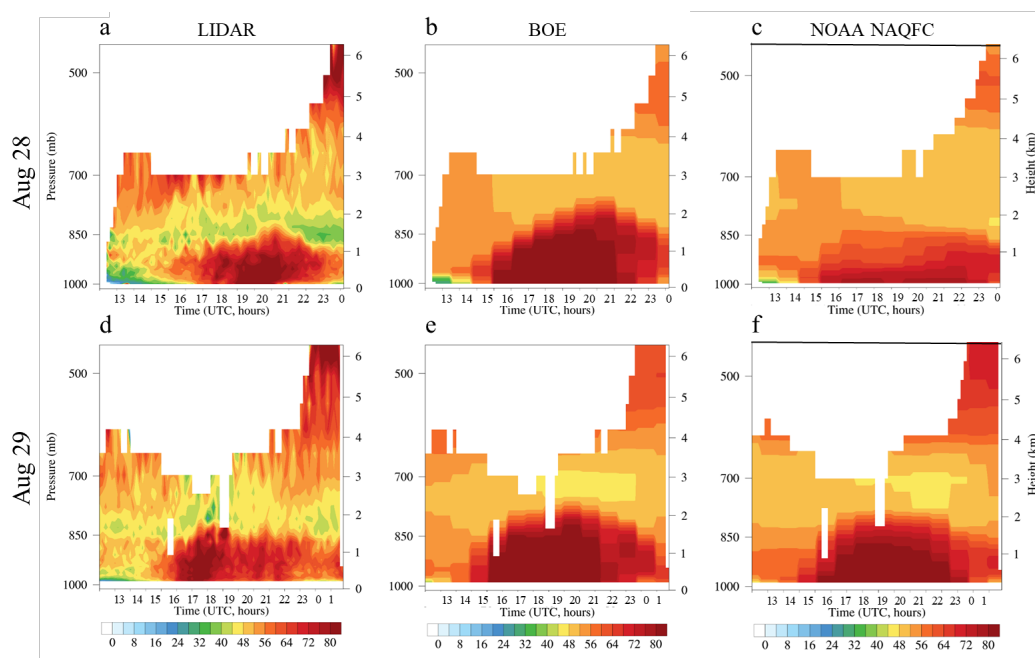


820 **Figure 11: Spatial distribution of NO<sub>2</sub> vertical column density (VCD) observed by NASA GeoCAPE Airborne Simulator (GCAS), and simulated by the 3 km BOE and 12 km NOAA NAQFC over the LIS domain during August 28–29, 2018. There were two flight missions each day: the morning flight (AM) from ~11:00 to 15:00 UTC and afternoon flight (PM) from ~16:00 to 20:00 UTC.**



825

Figure 12: Time series of observed and simulated surface  $O_3$  concentrations at the seven sites where the National Ambient Air Quality Standard (NAAQS) for  $O_3$  were exceeded during August 28–29, 2018: a. Colliers Mills; b. Riverhead; c. Greenwich; d. Madison-Beach Road; e. Middletown-CVH-Shed; f. Stratford; and g. Westport.



830 Figure 13: Vertical O<sub>3</sub> profiles (a) and (d) observed by NASA Langley Mobile O<sub>3</sub> Lidar (LMOL) and simulated by (b) and (e) the 3 km BOE and (c) and (f) 12 km NOAA NAQFC over the Westport site during (a)-(c) August 28 and (d)-(f) August 29, 2018. Note white represents missing data from LMOL.